Hydraulic Tomography and High-Resolution Slug Testing to Determine Hydraulic Conductivity Distributions – Year 4

The University of Kansas
Department of Geology

Brian J. Wachter
Carl D. McElwee
J. F. Devlin

Annual Report
SERDP
Strategic Environmental Research and Development Program
Project # ER1367
December 2008

Also
KGS Open-File Report no. 2008-23

Table of Contents

Background:

Considerable research has shown that the major control on the transport and fate of a pollutant as it moves through an aquifer is the spatial distribution of hydraulic conductivity. Although chemical and microbial processes play important roles, their influence cannot be understood without a detailed knowledge of the subsurface variations in hydraulic conductivity at a site. Many theories have been developed to quantify, in a generic sense, the influence of these variations using stochastic processes or fractal representations. It is increasingly apparent, however, that site-specific features of the hydraulic conductivity distribution (such as high conductivity zones) need to be quantified to reliably predict contaminant movement. Conventional hydraulic field techniques only provide information of a highly averaged nature or information restricted to the immediate vicinity of the test well. Therefore, development of new innovative methods to delineate the detailed hydraulic conductivity distribution at a given site should be a high priority. The research proposed here is directed at addressing this problem by developing techniques to map 3-D hydraulic conductivity distributions.

Objective:

Since spatial changes in hydraulic conductivity are a major factor governing the transport and fate of a pollutant as it moves through an aquifer, we focus on the development of new innovative methods to delineate these spatial changes. The objective of the research proposed here is to build on our previous work to develop and improve field techniques for better definition of the three-dimensional spatial distribution of hydraulic conductivity by using hydraulic tomography coupled with high-resolution slug testing.

Technology Approach:

We have worked for many years to quantify hydraulic conductivity fields in heterogeneous aquifers. One promising method we have worked on extensively is high-resolution slug testing. This method allows the delineation of the vertical distribution of hydraulic conductivity near an observation well. We propose to combine this method with another innovative method for investigating the hydraulic conductivity distribution between wells, called hydraulic tomography. We will use an oscillating signal and measure its phase and amplitude through space in order to estimate the hydraulic conductivity distribution of the material through which it has traveled. Our preliminary work shows that the phase and amplitude of the received signal can be measured over reasonable distances. The high-resolution slug testing results will be used as an initial condition and will provide conditioning for the tomographic inverse procedure, to help with any non-uniqueness problems. Slug test data are most accurate near the tested well and should probably not be extrapolated blindly between wells. Together, slug testing and hydraulic tomography should be more powerful than either one used alone and should give the best opportunity to characterize the hydraulic conductivity in-situ by a direct measure of water flow, as an alternative to indirect methods using geophysical techniques.

Introduction

A typical method used to determine fluid behavior in a geologic matrix near a well is a pumping test. Here a pump is installed into a well and groundwater is removed or injected while water levels in surrounding observation wells are monitored. Then the aquifer parameters can be estimated by monitoring changes in water levels at observation wells at some distance. These tests are typically large in scale, (Schad and Teutsch, 1994). Another test is an interference test, which is a special pumping test where the pump discharge has a variable rate. Interference tests are conducted by variable production or injection of fluid (hydraulic head changes) at one well, and observing the changing pressure or hydraulic head with time and distance at other locations. These tests are valued to estimate flow characteristics *in situ,* but are measures of the aquifer material over large volumes also.

On the other hand, physical cores of aquifer material can be obtained by various drilling methods. These samples can then be tested in a laboratory (i.e., falling or constant head permeability tests) to estimate the hydraulic properties. One advantage to this method is that the sample can be visually inspected. Some disadvantages to this method are that the material is disturbed from its natural environment and the sample is a small representation of the total aquifer.

Another common technique for determining aquifer parameters is slug tests. A slug test initiates a head change in a well, then monitors the response of the aquifer material to estimate the hydraulic conductivity (K). Slug testing is usually only conducted in a single well. It is generally accepted that the radius of influence of a slug test is small and only provides a limited view of subsurface hydrogeologic properties near

the well. Traditionally, slug tests have been initiated with the addition into a well of a known volume of water or a physical slug. More recently, pneumatic methods have become popular (Zemansky and McElwee, 2005; Sellwood, 2001; McCall et al., 2000) for multilevel slug testing. Slug tests in low K formations can take much longer than in material with high permeability. To overcome this, the fluid column in a well can be pressurized and the pressure change with time can be used as a alternative (Bredehoeft and Papadopulos, 1980).

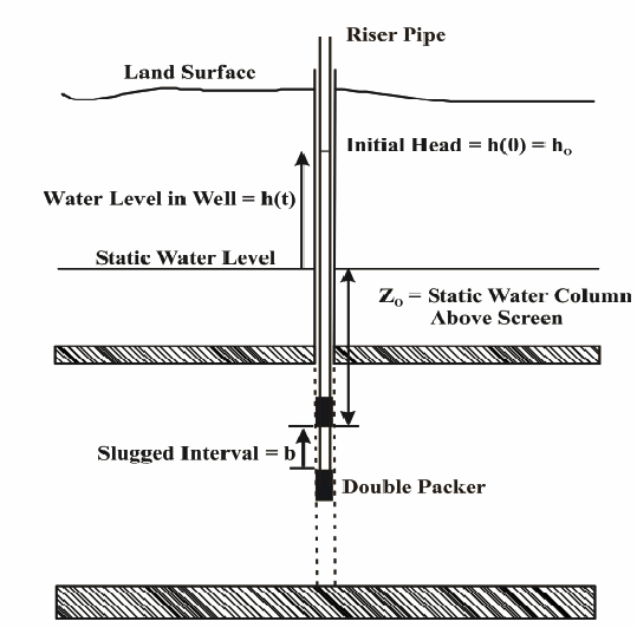

Figure 1. High resolution slug testing equipment deployed in a fully penetrating well.

Typical slug tests are conducted by exciting the entire length of the well screen. Whole well slug testing can provide information near the tested well but it is an average response over the total length of that well's screen. However, aquifers are naturally heterogeneous and whole well slug testing is unable to distinguish areas of high or low K. High resolution slug testing [(HRST), over short screen intervals (Figure 1)], provides a more detailed vertical profile of K near the tested well. In this research the HRST

interval is approximately 0.5 m; but, stressed intervals as small as 5 cm have been used (Healey et al., 2004). Currently there is no accepted method to bridge the gap between the larger lateral well-to-well averages from pumping or interference tests and detailed vertical estimates of K from HRST. Proposed here is a method to obtain estimates of aquifer parameters at larger radii of influence, while simultaneously maintaining a higher resolution.

Pulse testing is one method of determining fluid flow parameters that is often employed by the petroleum industry. Johnson et al. (1966) published results of experiments conducted in a sandstone reservoir near Chandler, OK. They found that the new pulse method was as effective as typical interference tests. The transient pressure signal is propagated by *in situ* fluid and is therefore a direct measure of reservoir diffusivity. Other advantages of the pulse method are the ability to distinguish the test from background noise because of its controlled frequency of oscillation and the reduction of down time relative to production. Since 1966, pulse testing has been used to delineate fractures (Barker, 1988; Brauchler, et al., 2001) and to predict water flood performance (Pierce, 1977).

Other pulse test examples include tidal, seismic, and oil field methods. The changes in groundwater levels as a result of tidal fluctuations have been well studied (Ferris, 1951; Hantush, 1960) and (Jiao and Tang, 1999). The sinusoidal tidal fluctuations that propagate inland through an aquifer are related to aquifer storativity and transmissivity. Solutions to water level fluctuations induced by seismic waves were presented by Cooper et al. (1965). The pressure head fluctuations controlling water levels are a result of the vertical motion of the aquifer but are dominated by dilation of

aquifer porosity. An interference test of alternating oil production and shut-in time was conducted to determine the interconnectivity of wells in a production field (Johnson et al., 1966). Here the source well is assumed to be a line source in an infinite homogeneous reservoir. The time lag and the received amplitude were used to estimate the average well-to-well transmissivity and storage properties of the reservoir. These oil field methods were theoretically adapted to hydrogeologic characterization by Black and Kipp (1981). Analytical solutions of a fracture responding to a single pulse interference test, a slug of water, was modeled and tested by Novakowski (1989). Straddle packers isolated the fracture and were used to apply the slug of water by being deflated. The duration of these tests was on average 30 min. The sequential pumping or removal of water was used to collect head responses between wells (Yeh and Liu, 2000). In these experiments multiple ray paths were analyzed as a hydraulic tomography experiment. Such experiments show promise in their ability to distinguish lateral and vertical 2-D variations in heterogeneity by changes in the signal over the travel path.

The research presented in this report uses continuous, controlled, sinusoidal pressure signals [the continuous pulse test (CPT)] as a means to estimate vertical profiles of well-to-well averaged hydraulic diffusivity. In this research, the primary method of stimulation of the alluvial aquifer was achieved by pneumatic methods. The column of air within a well was pressurized via an air compressor. A signal generator was used to open and close valves at the well-head allowing air to enter or exit the well. The signal generator produced an adjustable frequency step function, controlling the periodicity of the pulse-testing event. Theoretically, a square wave pressure test is the simplest to conduct because of the instantaneous pressure changes (Lee, 1982). Due to the input air

pressure, the water column in a well will be depressed creating flow through the well screen. This pulse of hydraulic pressure is transferred to the aquifer system based on the diffusivity of the material. As the air column within the well is allowed to return to atmospheric pressure, water rushs back into the well from the aquifer. These fluctuations are periodic and similar to tidal fluctuations acting upon a costal aquifer system. The governing equations for an aquifer responding to tidal fluctuations were adapted to Cartesian, cylindrical, and spherical coordinate systems describing groundwater flow with sinusoidal boundary conditions, in order to describe the data used in this report.

The period, the phase, and the amplitude of the produced wave can then be measured simultaneously at the source well and at observation wells. Through dispersion, the aquifer material will decrease the fidelity of a step input, retard the propagation, and attenuate the propagating wave front, resulting in a phase lag or shift, and a decrease in the amplitude. The amplitude ratio [received amplitude A_r divided by the initial amplitude A_0] and the phase difference [reference phase ϕ_0 minus the received phase ϕ_r] can then be used to calculate the hydraulic diffusivity (Lee, 1982).

Zero Offset Profile (ZOP, source and receiver at same elevation) data and Multiple Offset Gather (MOG, source location fixed; receiver elevation varied) data were collected at the University of Kansas' Geohydrologic Experimental and Monitoring Site (GEMS), a well-studied shallow semi-confined alluvial aquifer system in the Kansas River floodplain. Line sources equal to the total screen length and point sources isolated by custom bladder packers were used in these experiments. Field data indicate that sinusoidal signals can propagate reasonable distances, and may provide estimates of the

well-to-well diffusivity. Vertical profiles of hydraulic conductivity (K), measured with high-resolution slug testing (HRST), were collected for correlation with the CPT data.

The GEMS area is located in Douglas County, northeast Kansas, along the northern margin of the Kansas River flood plain (Figure. 2). GEMS is in a Pennsylvanian bedrock valley filled with Wisconsinan-age glaciofluvial terrace sediments (Schulmeister, 2000). The upper 11 m of sediments are mostly silts and clays and the lower 12 m of sediments at GEMS is a fining upward sequence of pebbles, coarse sand, and fine sand, underlain by the Tonganoxie Sandstone (Jiang, 1991). Within the sequences of sandy material are lenses of low permeability fine-grained sediments. These clay lenses occur at various elevations and can be up to 1 m thick (Schulmeister, 2000; Healey et al., 2004). As an aquifer, the Kansas River alluvium is a prolific deposit of unconsolidated sands and gravels. This high yielding semi-confined aquifer meets the needs of agricultural, industrial, and community interests.

Many studies have been conducted at GEMS and many well nests have been completed to various depths with various screen lengths. Porosity, grain size, and K were estimated by laboratory experiments performed on physical samples of the aquifer material (Jiang, 1991). A single-well injection tracer test was used to estimate a K distribution by monitoring the transport of an electrolytic solution (Huettl, 1992). The K distribution in an area of GEMS was also estimated by conducting an induced-gradient tracer test through a multilevel groundwater sampling well field (Bohling, 1999). Direct push bulk electrical conductivity (EC) profiling (Figure 3) and direct push pneumatic slug tests were also done adjacent to the tracer experiment well field (Sellwood, 2001).

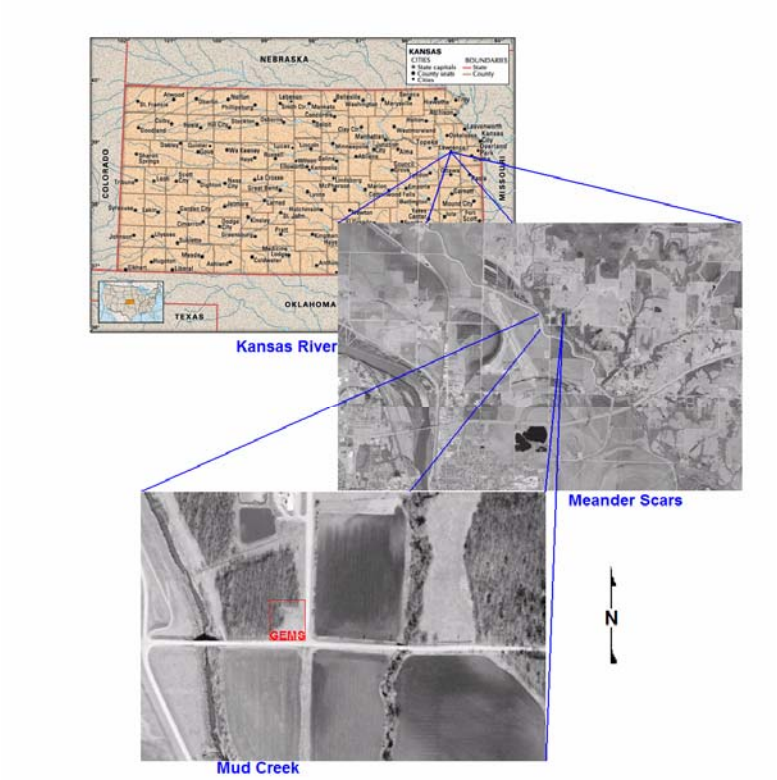

Figure 2. GEMS location map and aerial photographs.

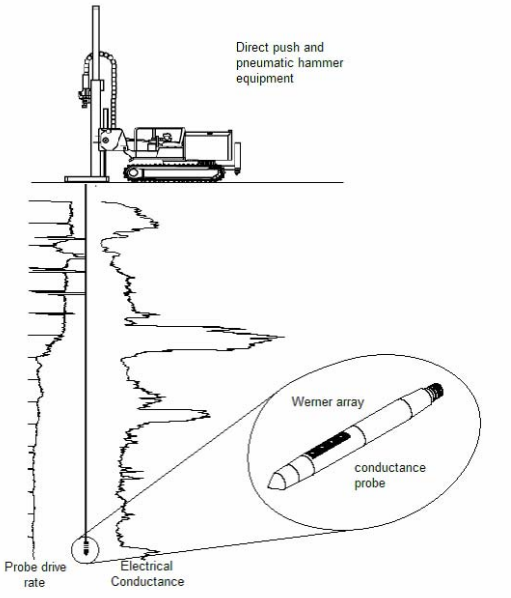

Figure 3. Direct push drilling unit, Electrical Conductance probe, and example profile.

Most recently, HRST K estimates were collected in numerous wells that were fully screened through the aquifer material (Ross, 2004; Ross and McElwee, 2007). These independent studies and the research presented here produced estimates of K that can be collected into a database. After compiling these data, vertical and lateral variations of the K distribution are evident. Typically at GEMS, K increases with depth in the sands and gravels, and low K material can be associated with high EC measurements, usually associated with the overlying silt and clay sediments. In most areas at GEMS, "layers" or zones of high K material are apparent in the sand and gravel aquifer.

Theory

Fluid flow in saturated aquifers behaves much like heat flow and can be described by similar equations. Excess pore pressures, matrix permeability, compressibility, and storativity all influence the fluctuations of groundwater levels in response to applied stresses. The excess fluid pressure P_e, above hydrostatic pressure P_s, is related to the total stress on the aquifer σ, and changes the stress $\Delta\sigma$ by

(1) $$\sigma + \Delta\sigma = \sigma_e + (P_s + P_e)$$

The above equation allocates the additional stress to either the aquifer matrix itself (σ_e) or to excess hydraulic pressure, P_e. By changing the hydraulic pressure or hydraulic head, the water levels in an aquifer also change accordingly. The total hydraulic head (h) hydraulic potential measured in a well is a combination of the elevation head z, and the hydraulic pressure head, P

(2) $$h = z + P/\rho g$$

such that

(3) $$P = P_s + P_e$$

Since the elevation is static, the only dynamic portion of h is due to pressure changes as shown in the following equation

(4) $$\frac{\partial h}{\partial t} = \frac{1}{\rho g}\frac{\partial P}{\partial t}$$

where ρ is the fluid density and g is the acceleration of gravity. Substituting equation (3) into equation (2) the total head measured in a well can also be expressed as

(5) $$h = z + (P_s/\rho_w g + P_e/\rho_w g)$$

Darcy's law states that the discharge Q of a fluid through a porous media depends on the hydraulic gradient (the change in head with distance) $\frac{\partial h}{\partial L}$, and the cross sectional area A. Darcy's Law is

(6) $$Q = -KA\frac{\partial h}{\partial L} \ .$$

Darcy's proportionality constant K, now called hydraulic conductivity, is a measure of how easily a fluid flows through an aquifer. By combining equation (5) with equation (6) the one-dimensional horizontal flow in the x direction q_x is

(7) $$q_x = -K_x\left(\frac{\partial h}{\partial x}\right) = -K_x\left(\frac{\partial}{\partial x}\right)\left[z + \left(\frac{P_s}{\rho g} + \frac{P_e}{\rho g}\right)\right]$$

Assuming that z and P_s are constant, the flow due to excess pressure is

(8) $$q_x = -\frac{K_x}{\rho g}\left(\frac{\partial P_e}{\partial x}\right)$$

Diffusivity is the ratio

(9) $$D = T/S = K/S_s.$$

D is a measure of the ability of an aquifer to transmit changes in the hydraulic head. The following conservation equations, written either in terms of P_e or h, demonstrate the relationship between K, S_s, and D

(10) $$K_x \frac{\partial^2 P_e}{\partial x^2} = S_s \frac{\partial P_e}{\partial t} \quad \rightarrow \quad D \frac{\partial^2 P_e}{\partial x^2} = \frac{\partial P_e}{\partial t}$$

and

(11) $$K_x \frac{\partial^2 h}{\partial x^2} = S_s \frac{\partial h}{\partial t} \quad \rightarrow \quad D \frac{\partial^2 h}{\partial x^2} = \frac{\partial h}{\partial t}$$

The above equations can be generalized to three dimensions. The goal of this research is to utilize the response of hydrogeologic material to cyclic pressure signals to estimate the D or K distribution in an aquifer.

Groundwater fluctuations near coastal regions have been studied and elementary equations have been developed to associate regional groundwater levels with tidal fluctuations (Hantush, 1960). The basic mathematical description of a one-dimensional transient pressure head signal with sinusoidal boundary conditions [$\sin(2\pi ft)$] is

(12) $$h(r,t) = h_o e^d \sin(\Phi_0 - \Phi_r).$$

The head at some distance and time h(r,t) is the initial amplitude h_o, some decay term e^d, multiplied by the sine of the source reference phase ($\Phi_o = 2\pi ft$) minus the phase shift, Φ_r. The amplitude decay and the phase shift depend on the ability of the aquifer to transmit the sinusoidal signal. Namely, it is the hydraulic diffusivity (D or K/Ss) of the aquifer that influences the hydraulic head measured at some distance and time from the source of a pressure head fluctuation. Three equations for the head response to the propagation of a sinusoidal boundary condition (causing excess fluid pressure) within a homogeneous

isotropic formation have been adapted from equation (12). Equation (12) has been extended to various coordinate systems, presented below.

Linear Cartesian System

(13) $$h(x,t) = h_o e^{-\sqrt{\frac{\pi f S_s}{K}}x} \sin\left(2\pi ft - \sqrt{\frac{\pi f S_s}{K}}x\right)$$

Cylindrical Radial System

(14) $$h(r,t) = h_o \frac{e^{-\sqrt{\frac{\pi f S_s}{K}}r}}{\sqrt{r}} \sin\left(2\pi ft - \sqrt{\frac{\pi f S_s}{K}}r\right)$$

Spherical Radial System

(15) $$h(r,t) = h_o \frac{e^{-\sqrt{\frac{\pi f S_s}{K}}r}}{r} \sin\left(2\pi ft - \sqrt{\frac{\pi f S_s}{K}}r\right)$$

Where t is time, x or r is the distance from the source, f is the frequency, h_o is the initial amplitude of the pressure head fluctuation at the source, S_s is the specific storage, and K is the hydraulic conductivity. Specific storage is the volume of fluid added or released per unit volume of aquifer per unit thickness, from compression or relaxation of the aquifer skeleton and pores due to changes in stress. The coordinate equations (13, 14, and 15) can be thought of as two parts: the amplitude [AMP] on the right hand side

(16) $$AMP = h_o \frac{e^{-\sqrt{\frac{\pi f S_s}{K}}r}}{r^*}$$

where r^* is the appropriate denominator in equations (13, 14, and 15), and the sinusoidal source phase Φ_o,

(17) $$\Phi_o = \sin\left(2\pi ft\right) \ .$$

The difference in phase Φ_r between two locations is expressed by the term

(18) $$\Phi_r = -\sqrt{\frac{\pi f S_s}{K}} r = d$$

which is equal to the exponential decay term (d) in equations (12, 13, 14, and 15). Both the amplitude decay and the degree of phase shift depend on the ratio of hydraulic conductivity to specific storage, which is the hydraulic diffusivity (D). Estimates of K may be inferred from equation (18) to compare with other methods if S_s is assumed.

The preceding equations can be used to predict phase and amplitude versus distance for homogeneous systems, where K and S_s are constant. However, for heterogeneous systems where no analytical solutions are available, one must resort to numerical solutions. We postulate that relatively simple formulas presented above can be used to analyze the data for heterogeneous cases by using a distance weighted average for the K. The premise is that the following replacement in the above equations might work.

(19) $$\sqrt{\frac{\pi f S_s}{K}} r \quad \Rightarrow \quad \sum_{i=1}^{I} \sqrt{\frac{\pi f S_s}{K_i}} (r_i - r_{i-1})$$

The index (I) indicates the present location of r; so, the summation continues up to the present location of r and terminates at that point.

As indicated above, one must resort to numerical methods to calculate the phase and amplitude relations with respect to distance for heterogeneous cases where K and Ss change with distance. We have developed numerical models for calculating the amplitude and phase in the presence of heterogeneity for Cartesian, cylindrical, and spherical coordinate systems. Previous year's annual reports (Engard et al., 2005; 2006)

showed that the simple replacement proposed by equation (19) can be used to simplify the inversion for K in certain cases. This year we have extended that investigation to the spherical heterogeneous system.

As shown above, the homogeneous equations can be used to predict K based on the measurable amplitude decay and phase shift. However, the values obtained for the horizontal rays must be interpreted as spatially weighted averages over the horizontal distance between wells. Equations (14) and (15) represent the two experimental approaches utilized in this research. The cylindrical radial equation (14) describes the behavior of the excitation of a relatively long and small radius section of screen that behaves as a line source. Fully penetrating wells are often constructed at GEMS. Any test where the total screen length is excited is termed a whole well test. The spherical radial equation (15) is a representation of the point source geometry, where the excited length of well screen is relatively short. To achieve this, either a partially penetrating well with a relatively short screen length or a straddle packer apparatus must be used. A straddle packer is a double inflatable packer arrangement, which isolates a centralized interval. It is advantageous if the packer apparatus can be deployed down typical 2 inch (5.08 cm) observation wells; so, considerable effort has been expended to design such packers for this research.

Previous studies have shown that a line source allows for higher energy input, higher amplitudes, and increased signal propagation (Black and Kipp, 1981). A line source can create multiple ray paths to the receiver, decreasing the resolution and only approximating gross K distributions. High K material can also preferentially propagate excess pore pressures generated by a line source, which will induce a vertical gradient

and cross-flow within the aquifer. Depending on the 3-D heterogeneity distribution, this cross-flow will alter the receiver signal, similar to a weighted average, again decreasing the resolution. Even high amplitude line source signals decay rapidly in the subsurface. Most of the decay is due to the exponential term in equations (14 and 15). In addition, the radial distance between source and receiver wells will cause further decay (the cylindrical or line source will additionally decay by the inverse square root of r [equation (14)] and the spherical or point source will decay by the inverse of r [equation (15)]). These additional amplitude decay effects are due to wavefront spreading loss. However, the point source arrangement may increase the resolution of the K distribution profile because of fewer ray path possibilities.

The common component of the amplitude decay and the phase shift is $\sqrt{\frac{\pi f S_s}{K}} r$; therefore, it is possible to compare the phase data to the amplitude data (after correcting for spreading loss). Using aforementioned assumptions, estimates of K can be obtained through algebraic manipulation. However, this method does not give a specific value for K, but rather an average ratio of S_s/K for the signal travel path from source well to receiver well. Simple theory presented here indicates that the phase and the corrected amplitude ratio should vary linearly with $\sqrt{\frac{S_s}{K}}$ and distance (r) from the source well. Therefore, average parameters between well pairs may be estimated. Further, if multiple source and receiver offsets (relative to their elevations) are used, multiple diagonal ray paths may be recorded (Multiple Offset Gathers, MOGs). This type of testing is called hydraulic tomography (Yeh and Liu, 2000; Bohling et al., 2003), and can give more detailed information about hydraulic properties between wells. In the first phase of this

project we concentrated on horizontal rays where the source and receiver are at the same elevation (Zero Offset Profiles, ZOP). A ZOP survey is the simplest tomographical survey to conduct and process, but can only give information on average horizontal aquifer parameters. During the second and third years of this project we started collecting diagonal ray path data (MOGs). These data show effects of heterogeneity in K. Therefore, we continue to expend considerable effort trying to find the optimum method of processing these field data.

Field Methodology

Recent studies at GEMS have utilized custom-built straddle packers (McElwee and Butler, 1995; Zemansky and McElwee, 2005; Ross and McElwee, 2007), and pneumatic slug testing technique techniques (McElwee and Zemansky, 2005; Sellwood, 2001; and Ross and McElwee, 2007). In this work custom made packers are used to isolate a zone for testing. This testing may either be high resolution slug testing (HRST) or cross-hole measurement of relative amplitudes and phases for hydraulic tomography .

HRST Techniques

The aquifer material at GEMS exhibits linear and non-linear responses to slug testing (Figure 4). The response of the aquifer material to the slug can be dampened such that water levels in a well return to static head conditions with time in a smooth non-oscillatory curve. However, the aquifer can be underdamped and water levels will oscillate, decaying with time, until pre-test conditions are reached (Van Der Kamp, 1976). Theoretical advances, presented by McElwee and Zenner (1998) and McElwee (2001, 2002), have made analysis of nonlinear behavior practical and meaningful. The

aforementioned slug tests are localized tests; but, continuous layers of geologic material between tested well pairs should correlate with HRST data from each well in the well pair.

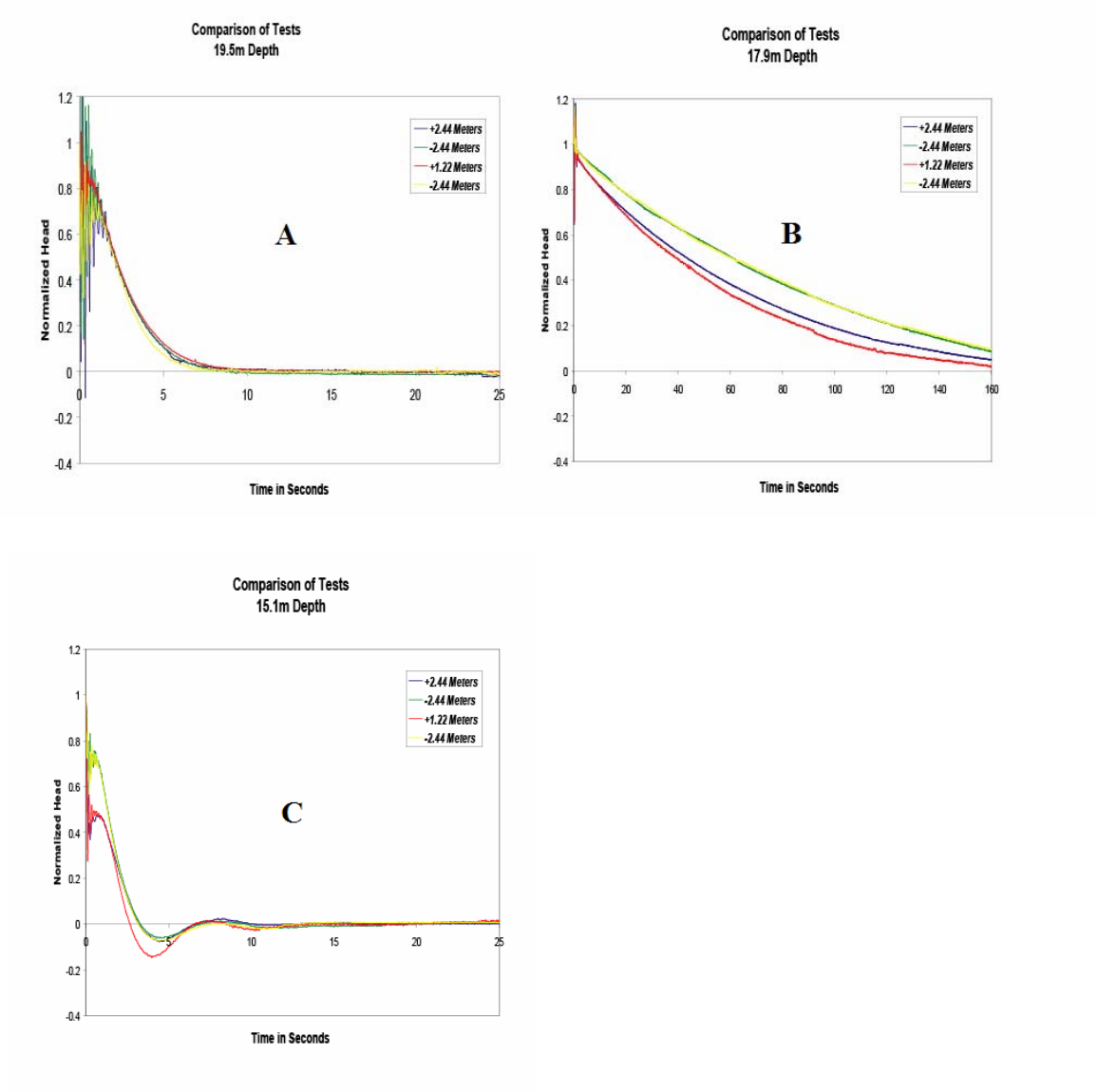

Figure 4. Three examples of slug tests performed at GEMS. Graph A displays no head dependence and behaves linearly. Graph B shows a dependence on the initial slug height and direction. Graph C is oscillatory and has some nonlinear characteristics.

CPT Techniques

The Continuous Pulse Test (CPT) is an exploratory method for extending slug test results between well pairs by propagating a sinusoidal signal. The distance between wells in pairs tested and analyzed with the CPT method in this research have ranged from 3 to 11.5 m. The instrumentation's ability to discern signal from noise may be a limiting factor at greater distances. As with most geophysical techniques, the equipment set up time can consume considerable time in the field. The pneumatic CPT method takes slightly longer to perform than the typical high resolution slug test.

An air compressor is used to supply the driving force behind the CPT method and it is connected to an apparatus attached to the top of the casing at the well (Figure 5).

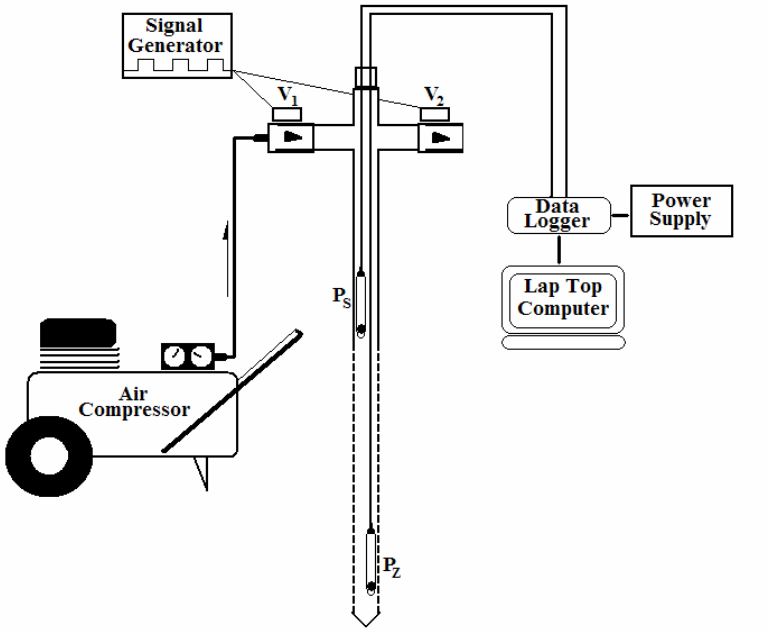

Figure 5. The pneumatic CPT equipment set up for a line source configuration. A signal generator opens and closes valves (V_1 and V_2) to control the flow of air supplied by the air compressor. The pressure transducers record the amplitude and phase at depth P_z and a reference location P_s. This setup can be easily modified for a point source configuration by using a double packer to isolate the stressed interval.

A signal generator is used to power servo-controlled valves on the apparatus, which allows air pressure to be increased in the well or to be released to the atmosphere. Increasing pressure depresses the water column, releasing the air pressure allows the water column to rebound. A single pulse of pressure is a slug test, while stacking them one after another, will create a CPT. The frequency and amplitude of the CPT data should be adjusted to give optimal results (Engard et al., 2005; Engard, 2006).

Surveys were done in the form of multiple offset gathers. For a MOG, a packed-off source excitation interval with a transducer is kept at a fixed depth in the source well while another packed-off receiver interval with a transducer is moved throughout the screened interval of the receiver well. For this study, measurements were usually taken in 0.30 m (one ft) intervals (sometimes 1.0 m or three ft intervals were used). After measurements were collected between one source location and all the receiver locations, the source was moved by 0.30 m and measurements were again collected at all the receiver locations. The process was repeated until rays had traveled from every location in the source well to every location in the receiver well (Figure 6). The collective examination of these multiple ray paths forms the tomographic study.

Initially, a single-channel receiver was used in data collection. However, a multi-level receiver with five pressure transducers was later constructed to expedite data collection. Pressure ports were located approximately 1 m apart isolated on either side by packers measuring approximately 0.6 m in length. The main advantage of this apparatus is that it allows efficient collection of multiple MOGs, which are needed for tomographic surveys.

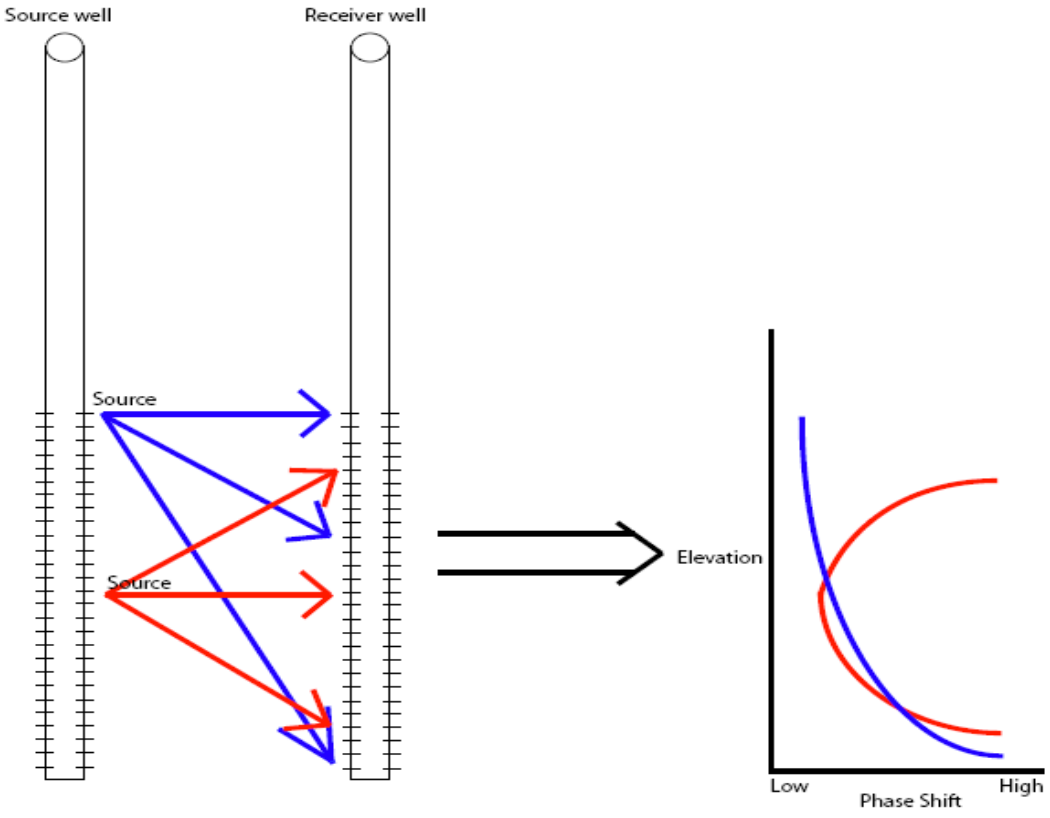

Figure 6. MOG setup for the tomographic study.

The MOG data taken from a well pair should produce a parabolic phase shift curve due to the path lengths of the rays. Path lengths are greater for more distant offsets (Figure 6). Larger phase and amplitude changes occur at these larger offsets. If the source is in the middle of the well, the greatest distance and therefore greatest change in amplitude and phase should occur when the receiver is at the top or bottom. The shortest distance is when the source and receiver are at the same depth. The general shape should be a parabola with distortions due to heterogeneity. When the source is at the top, the shortest distance is to the receiver location at the same depth and the greatest distance is to the receiver location at the bottom of the well. The curve should therefore have a half-parabola shape when the source is at the top of the well. The same is true when the

source is at the bottom of the well. Examples of these parabolic shapes are shown in Figures 6.

Pressure transducers were used to monitor pressure head fluctuations in both the source well and at the observation wells. The data were collected from the pressure transducers by a data-logger and stored on a field computer for later analysis. Data were typically recorded at a 20 Hz sampling rate, which provided sufficient temporal resolution. The field computer and data logger allowed real-time monitoring of the CPT records.

Vertical Sensor Array

We continue to improve the design of the vertical sensor array. Moving the receiver location to many discrete locations along the receiver well screen is very time consuming. To speed this process, we designed a vertical sensor array with 5 pressure transducers and 6 packers. Each transducer is isolated by packers above and below, to allow measurements to be made on a 0.3 m (1 ft) section of the receiver well screen. The transducers are located every 0.91 m (3 ft) along the array, with 0.6 m (2 ft) length packers between. The array may be moved up in 0.3 m (1 ft) increments two times to allow uniform coverage of the first section of the screen at 0.3 m (1 ft) increments. Nearly complete coverage of the 11 m screen can be achieved by pulling the vertical sensor array 3.9 m (13 ft) and repeating the sequence described above. In this way recording 6 records with the vertical sensor array is equivalent to 30 records with the single receiver setup. This increases the speed of data collection. Pictures of the vertical sensor array are shown below in Figure 7.

Figure 7. Vertical sensor array.

New Wells Installed

In late October 2007, three wells were added to GEMS. The wells were chosen to provide better coverage of the area under study by hydraulic tomography. The wells were installed using the direct push method with a Geoprobe unit from the Kansas Geological Survey. The wells initially installed for this project were HT-1, HT-2, and HT-3. The new wells are HT-4, HT-5, and HT-6. All of these wells and others previously used for hydraulic tomography work are shown below in Figure 8. After

installation and development, the wells were surveyed to establish the elevation of the top of each casing. Also, various radii between wells were measured for future analysis of the cross-well data. All of this information about the various wells that may be used in this tomographic study is shown in Table 1.

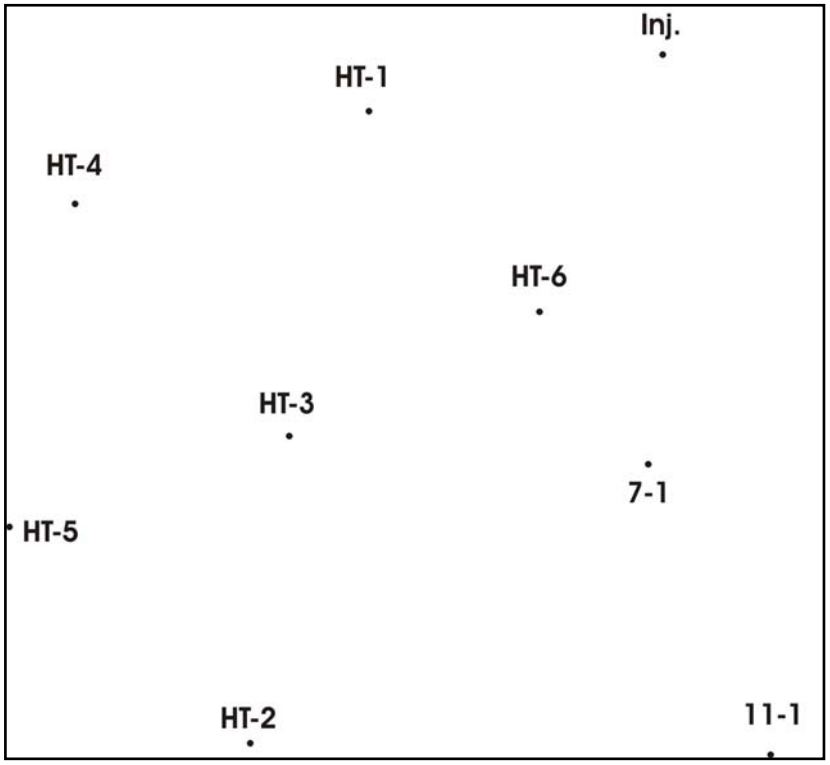

Figure 8. Relative well locations at GEMS (north is up). This shows the locations of the new wells installed in Oct. 2007, in addition to older wells previously used in this study.

Table 1. Well Information

Location	Elevation ft	Elevation m	Depth ft	Depth m	Screen ft	Screen m
Stake	827.556	252.239	-----	-----	-----	-----
HT-1	830.005	252.986	72.3	22.04	35.0	10.67
HT-2	829.66	252.880	72.4	22.07	35.0	10.67
HT-3	829.705	252.894	~70.	~21.3	35.0	10.67
HT-4	830.129	253.023	72.2	22.01	35.0	10.67
HT-5	829.651	252.878	71.9	21.92	35.0	10.67
HT-6	830.272	253.067	~72.	~21.9	35.0	10.67
7-1	828.342	252.479	68.85	20.99	30.0	9.14
11-1	828.358	252.484	69.40	21.16	45.0	13.72
Inj. Well	829.794	252.921	71.09	21.67	34.0	10.36

Well to Well Radial Distances, r

Well	Well	Radius (m)	Radius (ft)
HT-3 to	HT-1	4.77	15.65
HT-3 to	HT-2	4.36	14.31
HT-3 to	HT-4	4.46	14.62
HT-3 to	HT-5	4.21	13.81
HT-3 to	HT-6	3.99	13.10
HT-6 to	7-1	2.70	8.85
HT-6 to	11-1	7.19	23.58
HT-6 to	Inj. Well	4.04	13.26
Inj. Well to	HT-1	4.28	14.05
Inj. Well to	HT-4	8.67	28.45
Inj. Well to	HT-5	11.55	37.89
Inj. Well to	HT-2	11.49	37.70
Inj. Well to	HT-3	7.66	25.15
7-1 to	HT-2	6.94	22.79
7-1 to	HT-5	9.18	30.10
7-1 to	HT-3	5.13	16.84
7-1 to	HT-4	9.00	29.53
7-1 to	HT-1	6.46	21.20
HT-6 to	HT-1	3.79	12.42
HT-1 to	HT-4	4.40	14.44
HT-4 to	HT-5	4.63	15.21
HT-5 to	HT-2	4.57	15.00
HT-2 to	HT-6	7.40	24.28

Data Processing and Modeling

Data Processing

Data processing for the single-level receiver was done with FitAmpPhaseV8, a program written in Visual Basic by Carl McElwee. The program fits sine waves to the transducer data taken in the field and generates plots of the amplitude ratio and phase shift (x-axis) between the source and receiver transducers. All values are plotted against location (y-axis). The program analyzes data for a single source location at a time. For each MOG, the amplitude ratio and phase shift between the two source transducers should plot as a vertical line, as there is no change in material within the source well itself. The amplitude ratio and phase shift between the source and receiver should both plot as nearly parabolas or half-parabolas. If the source location is near the middle of the well, the shape will be a full parabola, and the shape will only be half a parabola if the source is near either the top or bottom of the well. The shape should be perfectly parabolic assuming no change in aquifer material, so any deviations from the overall parabola must be due to changes in K.

Data processing for the multi-level receiver was done with FitAmpPhaseV10HT, another program developed by Carl McElwee in Microsoft Excel using Visual Basic. This version of the program analyzes all five receiver transducers at once. Aside from accounting for multiple receiver transducers, the program is based on the same algorithms as FitAmpPhaseV8. Plots are generated for the receiver location versus both amplitude and phase shift. The raw data and the fitted sine wave for a single receiver location are shown below in Figure 9.

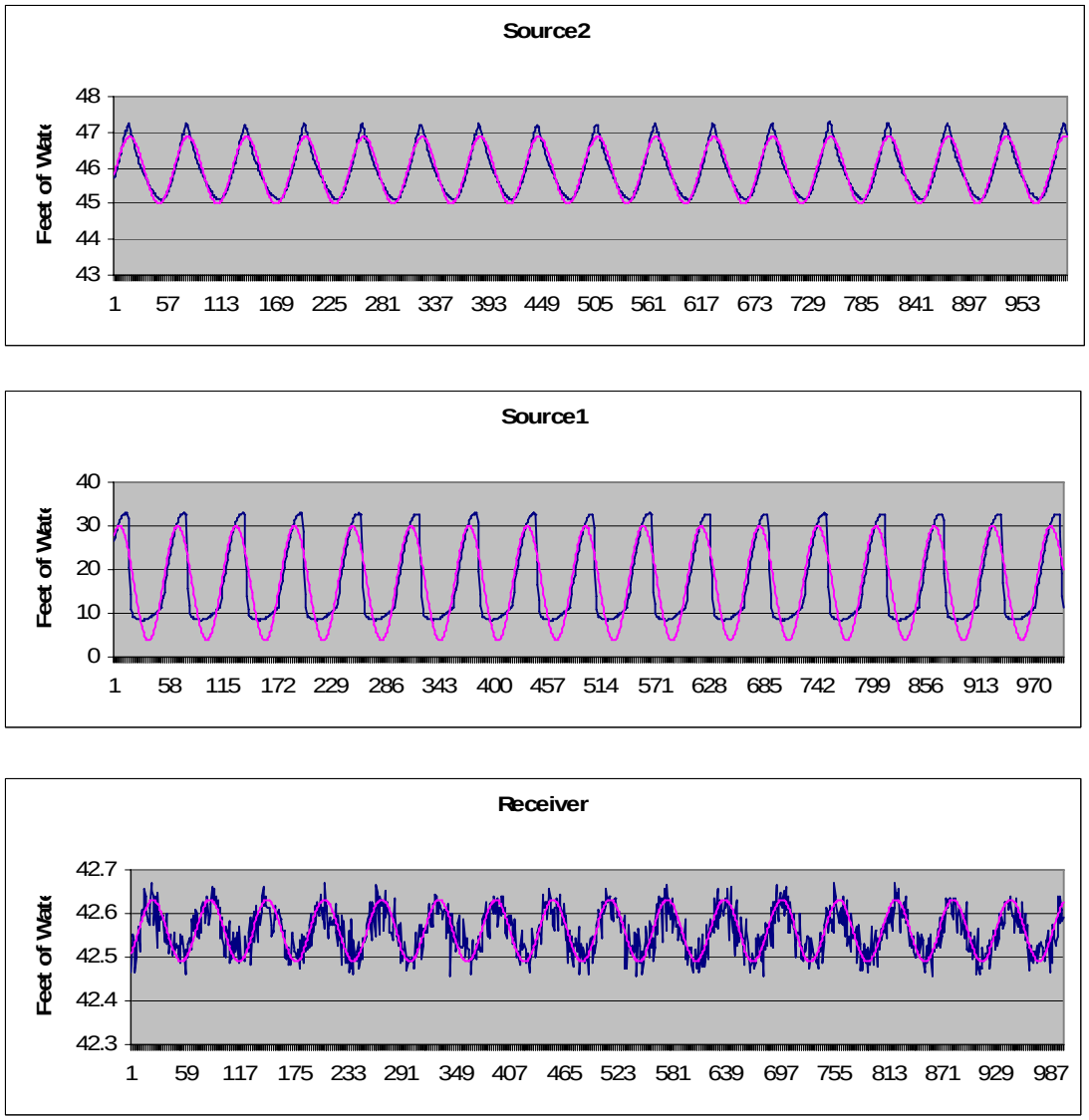

Figure 9: The data for one particular receiver location in the FitAmpPhaseV10HT program. Three plots are shown: one plot for each of the two source transducers and one plot for a receiver transducer. The raw data are shown in blue while the fitted sine wave is shown in pink.

High resolution slug test (HRST) data were processed using the program NLSLUG (McElwee, 2000), developed by Carl McElwee using Fortran and run from Microsoft Excel. Water and air pressure transducers are used to record the initial height of the slug test. For each record, a time break is chosen to begin measuring time, and static values at long times are determined for a base line. Multiple initial heads are used.

If the results are independent of initial head and behave linearly, all records lie on top of each other. Usually the records do not completely overlie one another, so there can be problems with both directionality, i.e. positive or negative initial head, and repeatability. Mobile fine sediments could explain both problems (McElwee and Zemansky, 2005). Slug testing can cause fine sediments to move, and these sediments may move more easily into the well than away from the well, creating an annulus containing more fine material at some radius. HRST data for the wells in this study were processed by Brett Engard and Pema Deki. The HRST results can be used to constrain the inversion to ensure that the interwell K values remain in the range observed in HRST results.

Modeling

Typical hydraulic tomography inversions use nonlinear least squares fitting and iterations to get the best fit, a process that can take much time and computing power. The procedure used for this paper uses spatially weighted ray paths. The path length in each zone of differing K is multiplied by a coefficient involving K to get the phase. Ray path data were generated by Hydraulic TomAnalV19, developed by Carl McElwee in Microsoft Excel. The field area was divided into a grid system with approximately evenly spaced divisions in the horizontal and vertical directions. Each box within the grid is referred to as an element. The model was divided into a series of nodes, elements, and grid spaces (Figure 10).

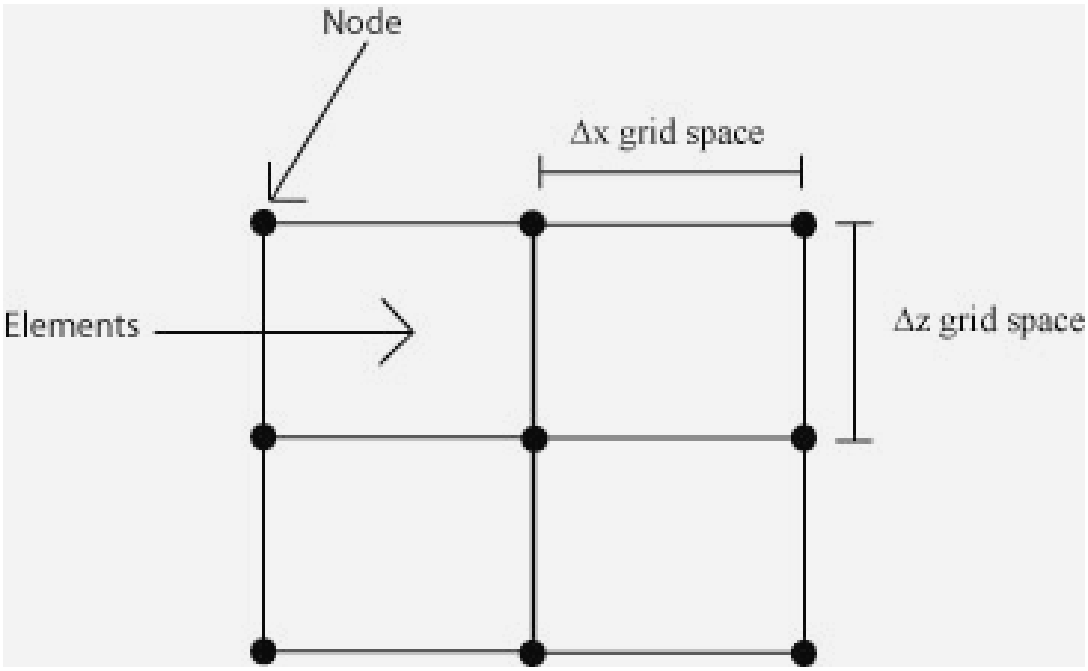

Figure 10: Depiction of a node, an element, and a grid space.

Nodes are any of the individual points throughout the grid. The vertical or horizontal spaces between two nodes, Δx and Δz, are known as grid spacing. An element is the rectangular area enclosed by four adjacent node points. The program computes the distance of each ray path through every element based on the Pythagorean Theorem. Path lengths through each element and phase shift values are then transferred to the LeastSquareSVDV13 program, developed by Carl McElwee in Microsoft Excel. The SVD, or Singular Value Decomposition, program performs a least squares fitting inversion from phase values to K values using a set of linear equations (Aster et al., 2005). Equations used in the program do not require iterations because they are linear. The SVD method divides G, an *m* (number of ray paths and equations) by *n* (number of zones and unknowns) matrix into the following equation:

$$G = UWV^T \qquad (20)$$

where U is an *m* by *m* orthogonal matrix, W is an *m* by *n* matrix with nonnegative diagonal elements known as singular values, V is an *n* by *n* orthogonal matrix, and the T superscript indicates that V is a transpose matrix.

Modeling studies were performed to compare results from the spatially weighted ray tracing method with those from a numerical model. The agreement between the numerical model and the spatially weighted ray trace method supports the transformation made back in equation 19. The application of the ray tracing method to simple models was reported in the previous year-end report. The conclusion was that the ray tracing method is an appropriate approximation for this work.

Theoretical values of phase and amplitude for more complex models were run through data processing programs before applying the programs to field data. The synthetic data set had no error built in. A model was set up with 6 grid spaces in the x direction and 10 grid spaces in the z direction, with 100 rays going through those 60 elements. The x distance was 19.2 feet and the z distance was 30 feet. K values were again chosen as 0.00182 m/s (0.006 ft/s) for the top and bottom layers and 0.000908 m/s (0.003 ft/s) for the middle layer, with the middle layer being the smallest layer. The value used for S_s was 0.00018. Instability problems resulted due to a difference in ray path density. The ray path density was highest in the center of the region, so there was less resolution at the top and bottom of the modeled area. The problem can be avoided by having spatially variable element sizes across the model. The top row of elements was combined into a single element and the bottom row was also combined into a single element, reducing the 60 element model to a 50 element model shown below in Figure 11. After combining the elements in those two rows, the model became stable and the

remaining section could still be resolved into blocks of about one meter on each side. The standard deviations on the K values were between 10^{-16} and 10^{-18}, implying that the inversion was almost perfect for the data with no noise.

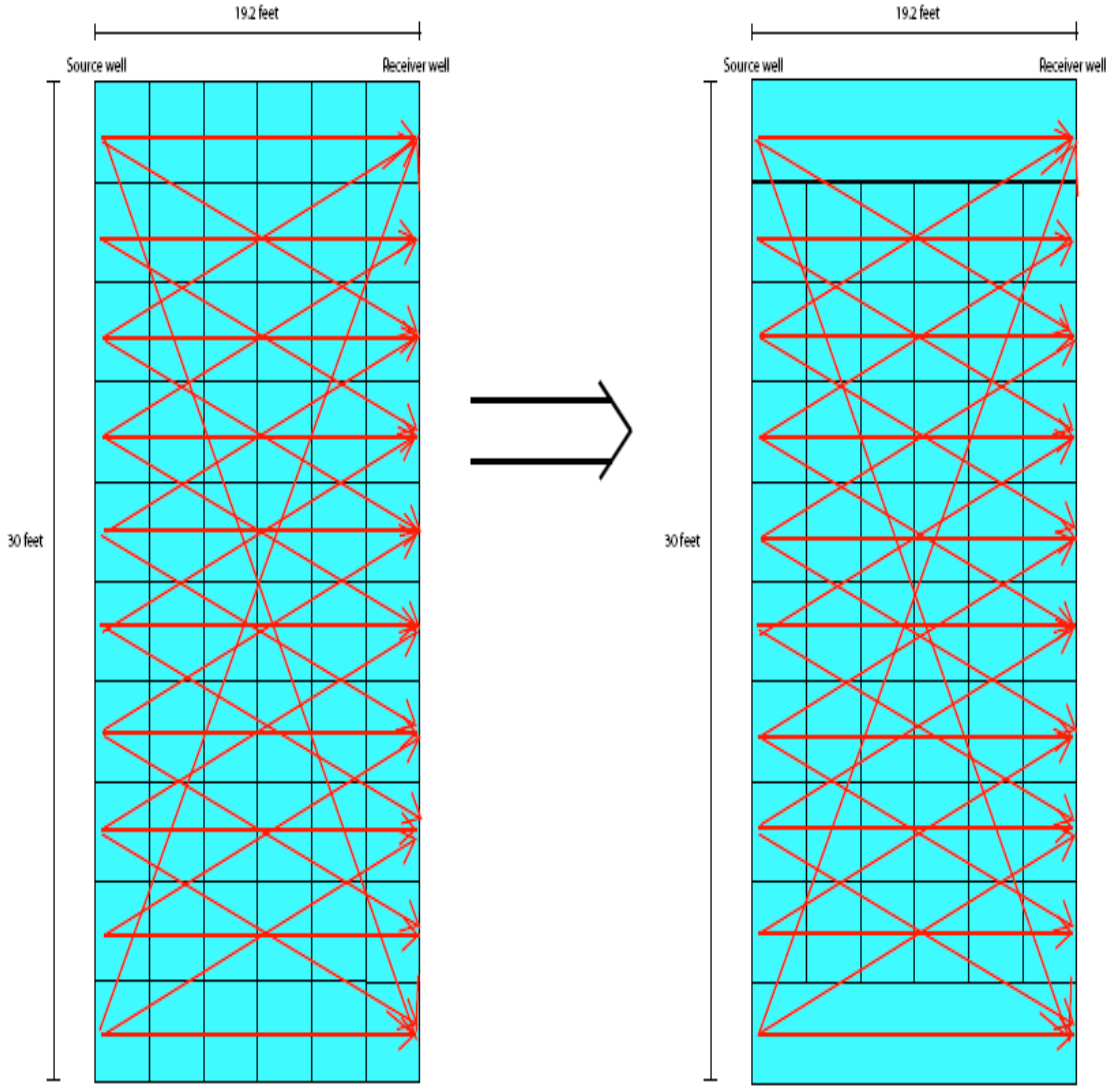

Figure 11: The 60 element model on the left was reduced to the 50 element model on the right to fix instability issues. Rays shown are conceptual and only represent a small portion of the total number of ray paths used.

Using a random number generator, values within the range of +/- 0.05 were added to the phase values. This translates to an error of +/- 5%, since the phase varies from 0 to

1. The 50 element model was again used since it had proven stable for the idealized data set. The model was unstable in each of five random error trials, with no consistent trend as to the location or magnitude of the unreasonable K values from the inversion. The model will continue to be refined to increase stability.

The model was also initially unstable when using the program on field data. The grid dimensions were slightly different than those of the theoretical data, but all sides of each element were still roughly one meter. This 36 element model used for the field data had 5 elements in the x direction and 9 elements in the z direction. The top row of elements was combined into a single element, and the bottom row was also combined into a single element. Instability problems still persisted, so the second row from the top and the second row from the bottom were each combined into single elements, as illustrated in Figure 12. After combining the first and last two rows, the model became stable and the remaining section could still be resolved into blocks of about one meter on each side, although a few K values were still outside of the range for GEMS as determined by previous studies. The anomalous K values necessitated additional modeling to increase stability and accuracy.

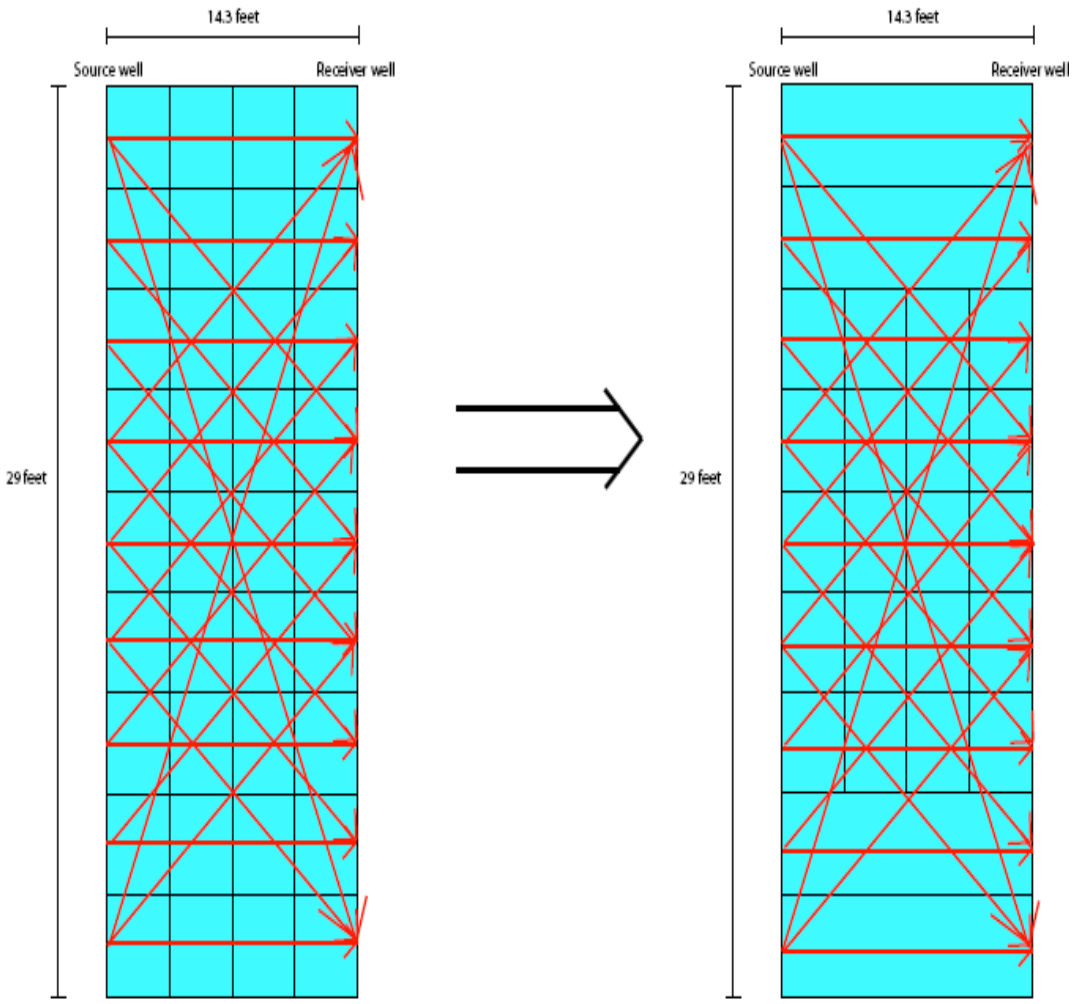

Figure 12: The 36 element model on the left becomes stable when reducing it to the 24 element model on the right. Rays shown are conceptual and represent a small portion of the total number of ray paths used.

The Hydraulic Tomography Analysis program was updated so that K could be specified by nodes rather than just by elements. Models were run to determine the optimal grid layout. The latest versions of the processing programs offer the ability to specify K by zones, which are formed by one or more nodes or elements and must be input manually. The purpose of the zones is to provide variable resolution across the model, with finer zones towards the center and coarser zones at the edges of the grid

where fewer rays are crossing. The current version of the SVD program also has the ability to perform Monte Carlo simulations, rather than running individual simulations for random error. The Monte Carlo simulations were run with both +/- 1% and +/- 5% noise for 1000 simulations. The variables investigated were: the number of nodes in the X direction (either 6 or 7), whether K was specified by elements or nodes, and the number of zones. The different combinations of input parameters resulted in 16 models. All initial models used 100 ray paths, consisting of 10 source locations and 10 receiver locations, and an S_s value of 0.00018. K values were arbitrarily chosen to start at 0.000914 m/s (0.003 ft/s) in zone 1 and gradually increased with depth to 0.00213 m/s (0.007 ft/s) in zone 16. Although the K values were arbitrarily chosen for the modeling phase, they fall within the range observed at the site (0.000305 m/s to 0.00305 m/s) from HRST and other methods. The results of the modeling studies are presented in Table 2 below in order of increasing average error based on 1% random noise.

The Hydraulic Tomography Analysis program calculates the length of each ray path through a particular element or nearby a given node. The total amount of length through each element or associated with each node was calculated by adding the lengths from each individual ray path of the 100 rays used. The ray path sums give a measure of the sensitivity of a given model to the K value in an element or near a node. These sums are presented below in Table 3. The sums are extremely small in the top and bottom rows, particularly for models where K is assigned to nodes. In the node cases, taking the whole first or last row as a zone still results in very small zone sums. The model was bounded by constant K nodes at each well based on HRST results. These constant values

do not contribute to the ray path sums, as indicated by the zeroes in the left and right columns in the node examples.

Table 2: Maximum and average error in K for a series of model input parameters (S_s = 0.00018) for two amounts of random noise.

K determined by	**# of X nodes**	**# of Zones**	**Max error - 1% noise**	**Avg. error - 1% noise**	**Max error - 5% noise**	**Avg. error - 5% noise**
elements	6	16	2.80	1.57	14.10	7.97
nodes	7	15	3.65	1.73	18.96	8.79
elements	6	20	2.67	1.75	14.18	9.12
elements	7	26	6.19	2.95	38.61	15.84
nodes	6	20	5.13	3.01	28.04	15.64
nodes	7	23	6.19	3.32	34.12	17.87
elements	7	24	10.11	3.58	103.08	21.60
elements	7	34	10.78	5.26	121.94	34.03
nodes	7	25	11.98	5.61	325.62	51.41
nodes	6	26	23.36	9.34	3156.65	406.65
nodes	6	24	22.98	9.72	3065.35	514.80
elements	6	34	18.52	10.29	2898.41	701.16
elements	7	52	41.37	17.49	3160.57	1465.70
elements	6	42	80.92	31.18	3145.44	1610.62
nodes	6	30	2868.10	1331.84	3160.65	2046.83
nodes	7	37	3159.82	1700.53	3145.48	1942.04

Table 3: Grid layout of ray path length sums in each element for the four models used (X = 4.36 m, Y = 8.84 m).

7 x 11 nodes (60 elements)

Elements

10.11	8.12	6.44	6.44	8.12	10.11
21.78	29.45	20.86	20.86	29.45	21.78
20.64	48.58	36.99	36.99	48.58	20.64
20.60	51.32	55.49	55.49	51.32	20.60
20.47	49.73	67.43	67.43	49.73	20.47
20.47	49.73	67.43	67.43	49.73	20.47
20.60	51.32	55.49	55.49	51.32	20.60
20.64	48.58	36.99	36.99	48.58	20.64
21.78	29.45	20.86	20.86	29.45	21.78
10.11	8.12	6.44	6.44	8.12	10.11

Nodes

0.00	4.13	2.16	1.78	2.16	4.13	0.00
0.00	27.62	15.47	13.45	15.47	27.62	0.00
0.00	43.33	33.24	27.95	33.24	43.33	0.00
0.00	45.70	49.68	44.86	49.68	45.70	0.00
0.00	44.45	57.43	63.04	57.43	44.45	0.00
0.00	43.94	58.43	72.23	58.43	43.94	0.00
0.00	44.45	57.43	63.04	57.43	44.45	0.00
0.00	45.70	49.68	44.86	49.68	45.70	0.00
0.00	43.33	33.24	27.95	33.24	43.33	0.00
0.00	27.62	15.47	13.45	15.47	27.62	0.00
0.00	4.13	2.16	1.78	2.16	4.13	0.00

Table 3: (Continued.)

6 x 11 nodes (50 elements)

Elements

10.22	8.73	7.73	8.73	10.22
24.86	31.02	23.90	31.02	24.86
26.56	53.88	42.95	53.88	26.56
25.64	65.29	64.59	65.29	25.64
25.04	65.72	85.47	65.72	25.04
25.04	65.72	85.47	65.72	25.04
25.64	65.29	64.59	65.29	25.64
26.56	53.88	42.95	53.88	26.56
24.86	31.02	23.90	31.02	24.86
10.22	8.73	7.73	8.73	10.22

Nodes

0.00	4.33	2.35	2.35	4.33	0.00
0.00	29.39	17.12	17.12	29.39	0.00
0.00	49.92	36.20	36.20	49.92	0.00
0.00	56.73	56.82	56.82	56.73	0.00
0.00	56.41	72.84	72.84	56.41	0.00
0.00	55.75	78.63	78.63	55.75	0.00
0.00	56.41	72.84	72.84	56.41	0.00
0.00	56.73	56.82	56.82	56.73	0.00
0.00	49.92	36.20	36.20	49.92	0.00
0.00	29.39	17.12	17.12	29.39	0.00
0.00	4.33	2.35	2.35	4.33	0.00

The amount of error produced by a given set of input parameters was balanced with the amount of resolution provided by that particular model. Increasing the number of zones increases the resolution, but only at the cost of increased error. The best compromise of error and resolution seems to occur somewhere in the middle of Table 2. Good resolution can be obtained with either 6 or 7 nodes in the X direction. For models with a comparable number of zones, there is less error when K is determined by elements. The 50 element model with 16 zones resulted in the least amount of error of the models studied here, but some models with more zones also produced acceptable amounts of error. The 34 zone model provides a good compromise between error and

resolution for the 60 element cases, while the 20 zone model provides a good compromise for the 50 element cases.

The 34 zone, 60 element model and the 20 zone, 50 element model discussed above produced too much error and instability when applied to the field data from the wells in this study. The problem was first investigated by using a model with only 5 nodes in the X direction, producing a 40 element model with 16 zones. Results were similar to those obtained with 50 elements with a comparable number of zones. The second variable investigated was S_s. Initial theoretical models used 0.00018 for S_s but changing to a more field appropriate value of 0.00001 resulted in consistent increases in the amount of error, as shown in Table 4. A good balance of error and resolution when S_s equaled 0.00001 was achieved with a 16 zone, 50 element model (6 X nodes). The average error was 7.79% in the presence of 1% noise. The 16 zone model with 6 X nodes will be used in all following discussions.

Table 4: Maximum and average error in K for a series of model input parameters ($S_s = 10^{-5}$) for two amounts of random noise.

K determined by	**# of X nodes**	**Zones**	**Max error - 1% noise**	**Avg. error - 1% noise**	**Max error - 5% noise**	**Avg. error - 5% noise**
elements	6	8	4.48	3.52	23.35	18.61
elements	6	10	8.83	4.96	66.94	30.25
elements	6	12	8.91	5.18	63.43	31.03
elements	6	14	12.32	7.11	489.26	128.90
elements	6	16	13.84	7.79	2975.59	533.84
elements	6	20	12.89	8.76	2876.63	381.94
elements	5	16	18.61	8.87	3087.28	664.41
elements	5	18	11.00	8.88	564.10	99.57
elements	4	16	15.19	9.92	3095.25	695.15
elements	5	22	23.02	13.70	3155.61	1277.53
elements	5	20	24.74	13.93	3160.06	1399.58
elements	5	26	25.50	14.63	3160.68	1265.16
nodes	6	20	25.38	14.87	3034.25	1377.35
elements	7	26	34.91	15.64	3153.50	1105.79

Similar to the sums presented by elements and nodes previously, the sum of ray path lengths going through each zone of the chosen model for the suite of rays used was also calculated. The grid layout is shown in Figure 13.

46	47	48	49	50
41	42	43	44	45
36	37	38	39	40
31	32	33	34	35
26	27	28	29	30
21	22	23	24	25
16	17	18	19	20
11	12	13	14	15
6	7	8	9	10
1	2	3	4	5

Figure 13: The grid shows the division of elements into 16 zones.

In Figure 13, each of the 50 elements is numbered, with element 1 at the bottom of the source well and element 50 at the top of the receiver well. The greatest resolution is provided in the middle of the grid while the top and bottom have the least resolution. The zone sums presented below in Figure 14 were calculated using field geometry and the actual number of rays collected in the field for each well pair, and they represent a measure of the sensitivity of the model to the K value in each zone.

In each well pair, the center of the model prior to zoning had the highest sum of ray path lengths because the most ray paths passed through those areas. Other nodes or elements were combined together to produce zones with sums comparable to the value in the center. Zone sums may differ by a factor of two but should not vary by as much as an order of magnitude. Zone sums in a given zone are fairly similar between well pairs with

approximately the same number of ray paths. Variation occurs from one well pair to another partially due to differing radii but largely due to the changing number of ray paths.

(a). HT-3 to HT-2 (750 rays)

823.77		
1228.00		
630.15	405.42	537.70
667.15	548.02	523.73
664.30	546.10	526.06
616.21	404.27	545.03
1213.79		
820.19		

(b). HT-3 to HT-1 (780 rays)

1154.96		
1434.27		
691.30	472.55	597.74
707.20	612.89	585.77
704.63	580.72	591.74
651.07	416.50	605.51
1278.80		
807.51		

(c). HT-4 to HT-3 (100 rays)

139.51		
166.25		
75.58	52.77	75.72
75.27	72.18	75.30
75.07	73.41	75.05
75.94	54.72	75.81
170.54		
152.43		

(d). HT-5 to HT-3 (190 rays)

143.02		
211.02		
150.46	71.51	75.04
148.99	124.07	102.38
140.86	144.98	160.69
136.40	123.90	199.25
403.52		
362.43		

(e). HT-6 to HT-3 (300 rays)

361.10		
454.76		
209.34	143.64	214.51
211.15	202.04	212.24
211.16	210.42	209.94
216.29	158.90	211.12
487.74		
456.77		

Figure 14: The sums of ray paths in each zone for well pairs HT-3 to HT-2 (a), HT-3 to HT-3 (b), HT-4 to HT-3 (c), HT-5 to HT-3 (d), and HT-6 to HT-3 (e).

Results

SVD Processing

After choosing a zoning model, field data were run through the inversion program to determine K values. As stated in the Modeling section, the model chosen for this scenario was a 16 zone model where K was determined by elements and there were 6 nodes in the X direction. The data set from well HT-3 to well HT-2 was first examined because it seemed to be the best of the initial data sets. The HRST K values determined in previous tests were input as constant K nodes to help fix the other K values within a reasonable range. HRST results were processed by Brett Engard for wells HT-1, HT-2, and HT-3, and by Pema Deki for wells HT-4, HT-5, and HT-6.

Contour plots were made of K values plotted against elevation and the radial distance between wells using a program called QuikGrid, a public domain program. The program contours between points written in an x,y,z format, in this case corresponding to radius, elevation, and K. The contour interval chosen is 0.0002 m/s. The HRST values were chosen for the K values at each well in the plot. Interwell K values were determined by the SVD analysis, a method using least squares. In the contour plots of K, the source well is on the left side and the receiver well is on the right side.

Initially the field data were processed using an unconstrained SVD procedure. The results were unstable with regions of K occurring that were known to be unreasonable. The SVD inverse program performs perfectly on model data without noise, so it must be much more sensitive to noise than originally thought. To compensate for the sensitivity to noise, a seven point filter was used on the data. In addition, noise reduction was attempted by editing larger offset rays, where noise was expected to be

greater. Little improvement was observed due to filtering and ray path editing. Apparently, the inverse procedure needed some additional conditioning to become stable. As an alternative processing scheme, an SVD least squares fit was employed constrained by the HRST data, which is detailed in the following section.

Constrained SVD Results

Inverse problems are commonly constrained with data known from other sources or methods; in this case, HRST results were used to constrain the inversion for K values. Initial guesses of K in each zone were obtained through a linear interpolation of HRST values at the same Z elevations. The sum of squared errors (SSE) was calculated by comparing the phase values measured in the field to the phase values calculated using SVD. A weighting factor is used in the latest version of the SVD program to determine to what extent the HRST results constrain the inversion. A weighting factor of zero is equivalent to the unconstrained SVD analysis, and increasing values for the weighting factor result in increasing weight given to the HRST results and therefore less deviation from HRST values. For this study, a weighting factor of 1.0 was used, resulting in about equal weight of the HRST data and the tomographic data. The K value in a zone is only changed if it is still in the approximate range of values seen from HRST. The results were calculated using two values for S_s, 10^{-5} (Table 5) and 1.5×10^{-5} (Table 6).

Table 5: K values (m/s) obtained after iterating using the constrained SVD analysis ($S_c = 10^{-5}$).

Zone	HT-3toHT-1 50elem 780 rays	HT-3toHT-2 40elem 750 rays	HT-3toHT-2 50elem 750 rays	HT-3toHT-2 50elem 270 rays	HT-3toHT-2 50elem 170 rays	HT-3toHT-2 50elem 90 rays	HT-4toHT-3 50elem 100 rays	HT-5toHT-3 50elem 190 rays	HT-6toHT-3 50elem 300 rays
1	0.004404	0.0074862	0.0058252	0.0051154	0.0051625	0.0049338	0.0060699	0.005425	0.0107446
2	0.0011044	0.0007794	0.0012579	0.0011813	0.0015434	0.0012734	0.0014829	0.0009898	0.001248
3	0.0003231	0.001476	0.0006166	0.0005975	0.0007826	0.0006126	0.003498	0.0027994	0.0037067
4	0.0004029	0.0012684	0.0010956	0.0010228	0.0010677	0.0010214	0.0024315	0.0020906	0.004816
5	0.0003207	0.00413	0.0012579	0.001162	0.0013765	0.0011777	0.0015143	0.0007947	0.0033531
6	0.0067165	0.001326	0.002753	0.0028131	0.0024481	0.0025694	0.0033182	0.005046	0.0158121
7	0.0018712	0.002018	0.0017516	0.0016532	0.0017923	0.001771	0.0065138	0.000976	0.0023381
8	0.0020057	0.0064817	0.0052522	0.0041009	0.004814	0.0036683	0.0079078	0.003463	0.0061995
9	0.0017238	0.0054021	0.0016193	0.0017939	0.0014134	0.0016523	0.0053158	0.0013502	0.0031366
10	0.0010119	0.0013811	0.0010374	0.0009865	0.0010515	0.0009151	0.007074	0.0005979	0.0012969
11	0.0019704	0.0022031	0.0035885	0.002996	0.0027921	0.0033401	0.0074449	0.00148	0.004094
12	0.0011519	0.0037096	0.0022713	0.0022118	0.0015644	0.0019312	0.0047499	0.0007769	0.001627
13	0.0012693	0.0026868	0.0031371	0.0032096	0.0032301	0.0027179	0.0040592	0.0019252	0.003049
14	0.0009069	0.0023642	0.0030193	0.0027131	0.0034024	0.0031891	0.0051039	0.0016292	0.0030399
15	0.0006855	0.0015154	0.0015675	0.0014628	0.0012573	0.0013588	0.005706	0.0004734	0.0007758
16	0.0004172	0.0014292	0.001563	0.0014545	0.001413	0.0013843	0.0040793	0.0005685	0.0004313

Table 6: K values (m/s) obtained after iterating using the constrained SVD analysis ($S_s = 1.5 \times 10^{-5}$).

Zone	HT-3toHT-1 50elem 780 rays	HT-3toHT-2 40elem 750 rays	HT-3toHT-2 50elem 750 rays	HT-3toHT-2 50elem 270 rays	HT-3toHT-2 50elem 170 rays	HT-3toHT-2 50elem 90 rays	HT-4toHT-3 50elem 100 rays	HT-5toHT-3 50elem 190 rays	HT-6toHT-3 50elem 300 rays
1	0.0059224	0.0110622	0.0083746	0.0074443	0.0078103	0.0073452	0.0098291	0.0081054	0.0165329
2	0.0018614	0.0010535	0.0019261	0.0018041	0.0023823	0.0019379	0.0019216	0.0014876	0.0016687
3	0.0003661	0.0020754	0.0007449	0.0007199	0.000909	0.0007349	0.004419	0.0037312	0.0049737
4	0.0004441	0.0017475	0.0013065	0.001226	0.001314	0.0012316	0.0028086	0.0026506	0.005839
5	0.0003943	0.0046685	0.0016376	0.0015258	0.0018896	0.0015556	0.0017495	0.0010506	0.0042925
6	0.0117715	0.0019606	0.0042273	0.0042145	0.0036413	0.0038003	0.0041749	0.0069156	0.0225553
7	0.0029366	0.0028427	0.0026044	0.0024617	0.0026194	0.0026404	0.0091596	0.0014505	0.0034871
8	0.0030084	0.0068331	0.0073598	0.0057864	0.0067727	0.0051398	0.0112893	0.0051215	0.0084238
9	0.0024074	0.0063557	0.0021918	0.0023827	0.00192	0.0022097	0.0070657	0.0017724	0.0037579
10	0.0014646	0.0020357	0.0014203	0.0013562	0.0014085	0.0012542	0.0098941	0.0008195	0.0018103
11	0.0028141	0.0030217	0.0045188	0.003851	0.0033914	0.0042758	0.0103932	0.0018801	0.0056214
12	0.0016502	0.0039212	0.0032263	0.0031156	0.0022854	0.0027373	0.0060878	0.0011181	0.0021965
13	0.0016482	0.004098	0.0040081	0.004086	0.0039623	0.0034614	0.0047432	0.0024411	0.0039505
14	0.0012285	0.0033796	0.0042178	0.0038217	0.0043313	0.0044617	0.006579	0.0021453	0.004361
15	0.0010405	0.0021742	0.0023255	0.00217	0.0018061	0.0019993	0.008918	0.0007141	0.0011548
16	0.0006021	0.001872	0.0021013	0.0019843	0.001795	0.0018571	0.0052272	0.0007761	0.0006102

Contour plots were made of K values plotted against elevation and the radial distance between wells for the data constrained by the HRST results. The HRST values are used at the left and right ends of the plot, with the source on the left and the receiver on the right. Interwell K values in the following plots were all determined by the constrained SVD analysis. The phase is a ratio between S_s and K, so changes in S_s will also result in changes in K. This introduces a potential source of error because, due to the difficulty of measuring S_s in situ, a value was obtained from the literature rather than from field measurements. To investigate the effect of S_s, the constrained SVD analysis was conducted on all of the data using S_s values of both 10^{-5} (Figures 15-22) and 1.5 x 10^{-5} (Figures 23-30). A value of 1.5 x 10^{-5} in general results in smoother transitions between zones. The negative aspect of choosing the higher S_s value is that well pair HT-6 to HT-3, which already had higher than expected K values with the lower S_s (Figure 22), continues to increase above the expected range (Figure 30).

Based on other work at the site, and in particular HRST, K values at the site are known to range from approximately 0.0003 m/s up to 0.003 m/s. The K values in figures 15 and 23 are all within this range. The trend also matches that seen in HRST results, with low K material near the top, a high K region in the middle, another high K region beginning at the bottom of the plot, and a low K zone between the two high K regions. The data set from HT-3 to HT-2 was used to verify that the program was working correctly before extending the analysis to other well pairs. Figure 23, using a value of 1.5 x 10^{-5} for S_s, shows a smoother transition between points than Figure 15, which is physically a more likely scenario.

Plots were also made of the HT-3 to HT-2 data set using less than 750 rays to determine if fewer rays can provide the same results. The number of rays in each example was based on the ray path geometry of the other well pairs. The 270 ray path example used all receiver data for each source used but only every third source location, just like well pair HT-6 to HT-3. Similarly, the 170 ray path example followed the same pattern as well pair HT-5 to HT-3 and the 90 ray path example followed the pattern of well pair HT-4 to HT-3. The three following figures (Figures 16-18) show the same trend seen in Figure 15, but the magnitudes of the K values decrease as the number of ray paths decreases. The 270 ray path scenario (Figure 16) is closest to the 750 ray path scenario. The bottom zone is about the same in the 750 and 270 ray path cases, but the K values in the bottom zone are noticeably smaller in the two cases with less ray paths. The plots using the higher S_s value (Figures 24-26) also show the same trends, but the transitions between zones are smoother.

The data set presented in Figure 19 is not as accurate as the other data sets. The amount of error between calculated and observed phases was greater than that in other well pairs. Problems with this data set are likely caused by the nitrogen leaks at the time of data collection. The equipment was repaired after this data set was completed. In spite of the problems, the plot shows the same general zones of high and low K seen elsewhere. Figure 27, using the larger Ss value, depicts the same zones of high and low K. The processing program is probably not causing the problems because it has been constrained and other well pairs do not have as many problems. So, drawing definite conclusions about this well pair would likely require recollecting the data with the current repaired equipment.

Both of the original well pairs verified the use of the constrained processing program by showing the trends observed in HRST results, so the data from fall 2007 were examined for the three newest wells. The vertical intervals were varied in the source and receiver wells for some of the wells pairs; this offered the opportunity to determine if data were being collected at adequate spatial intervals for appropriate resolution. The data in figures 20 and 28 show the overall trend observed between HT-3 and HT-2 and between HT-3 and HT-1. Once again, the plots demonstrate the expected trends of high and low K zones. The high K zone near the top of the plot is not seen elsewhere in that portion of the aquifer, but the values are at least within the overall range determined by other methods. This could potentially be caused by a combination of previously discussed problems of resolution in the top of the sampling area in combination with the low number of ray paths used for this particular well pair (100, compared to 750 for HT-3 to HT-2).

The results between well HT-5 and well HT-3 are presented in Figures 21 and 29. The difference between the two figures is that the transitions between K values are smoother in the plot using the higher value for S_s. Some of the values at the bottom of the plot are slightly above the general expected range, but still within reason. K values have been shown to slightly exceed 0.003 m/s in some of the HRST data toward the bottom of the wells. The same trend of low K material at the top, a moderately high K zone in the middle, and high K material at the bottom is again observed in this well pair. As with the plot from well HT-4 to well HT-3, the relatively large region of very low K values at the top could be due to the lower number of ray paths for this well pair.

The contour plots from well HT-6 to HT-3 (Figures 22 and 30) show the same trend seen in tomography experiments between all the other well pairs, as well as in HRST results. The zone of very high K in the middle left side of the plot exceeds the range of expected values for the site. The location of the zone could be due to the survey design for this well pair, namely, the source locations were sampled at a coarser interval than that used for the receiver locations. This well pair is the only one examined in this study for which increasing S_s resulted in K values farther above the expected range. Despite the problem of larger than expected K values, the transitions between zones are again smoother using 1.5×10^{-5} instead of 10^{-5} for S_s.

The number of ray paths collected for a well pair correlated well with the reasonableness of the K values. The well pair with the best results, HT-3 to HT-2 (750 rays) was characterized by the most rays of any of the well pairs, with the exception of the well pair with equipment problems. The well pairs of HT-4 to HT-3 and HT-5 to HT-3 had 100 rays and 190 rays, respectively, and some of the higher elevation zones were somewhat lower than expected for the site. The results suggest that 190 ray paths are not enough for accurate results. Time constraints may not always allow for 750 ray paths, but there does seem to be a strong correlation with the accuracy of the processing results and the number of ray paths. The work with editing ray paths for the data set from HT-3 to HT-2 also lends support for collecting as many ray paths as time permits. The resolution of K values decreased as more rays were edited out. Although it takes less time to collect 300 ray paths than to collect 750 ray paths, the additional rays will provide some increase in accuracy.

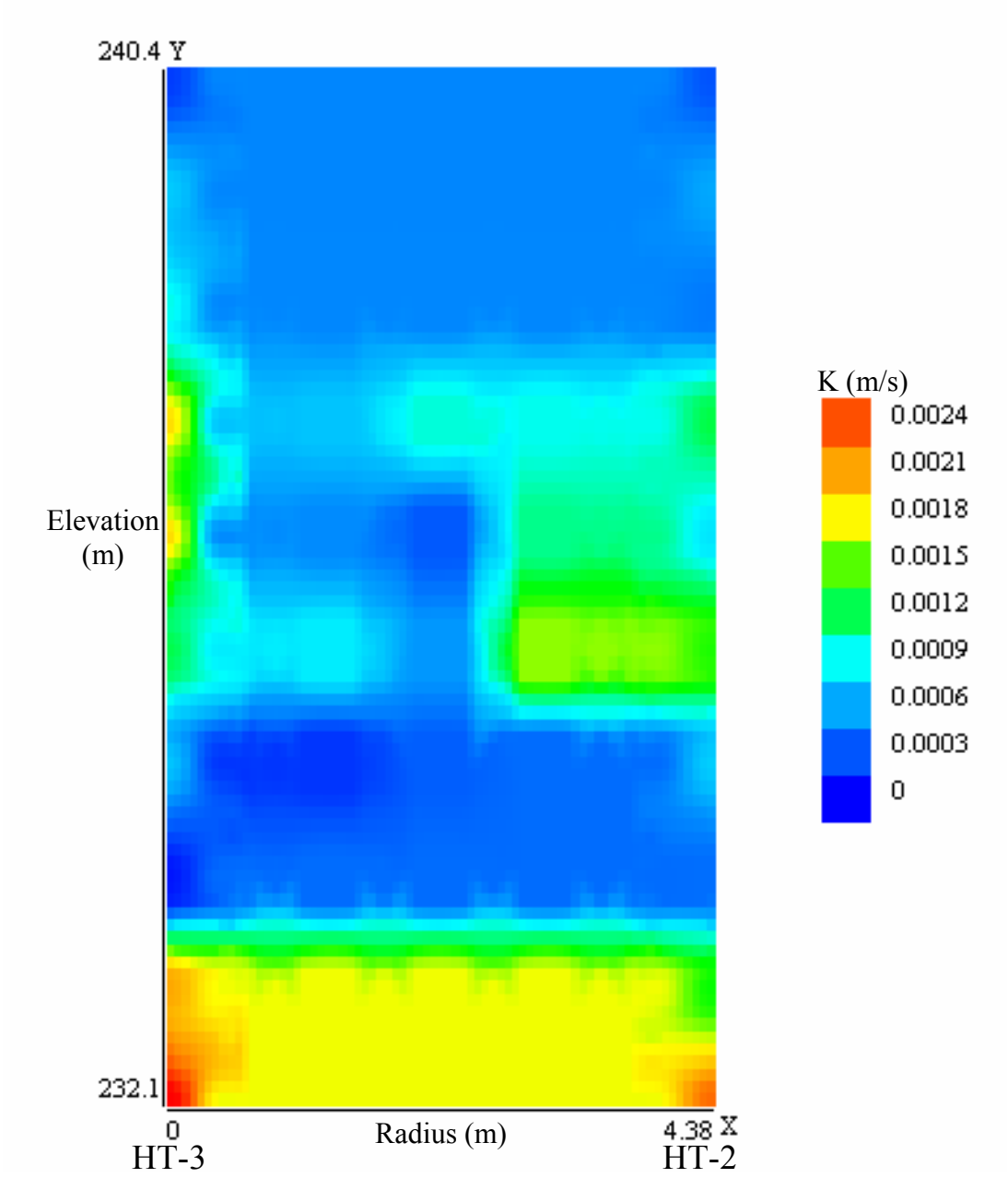

Figure 15: Interwell K values from constrained SVD analysis with HT-3 as the source well and HT-2 as the receiver well (750 rays, $S_s = 10^{-5}$).

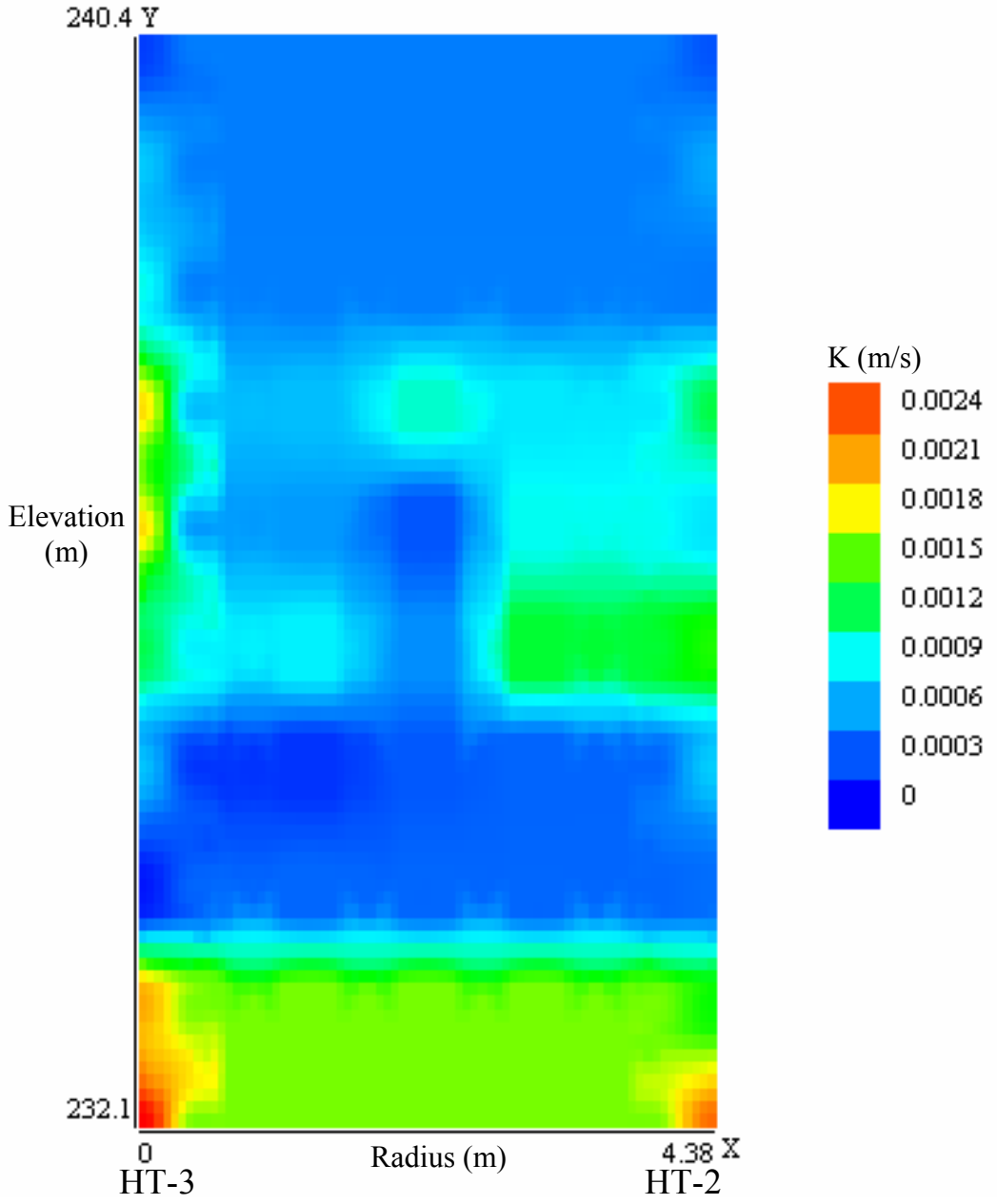

Figure 16: Interwell K values from constrained SVD analysis with HT-3 as the source well and HT-2 as the receiver well (270 rays, $S_s = 10^{-5}$).

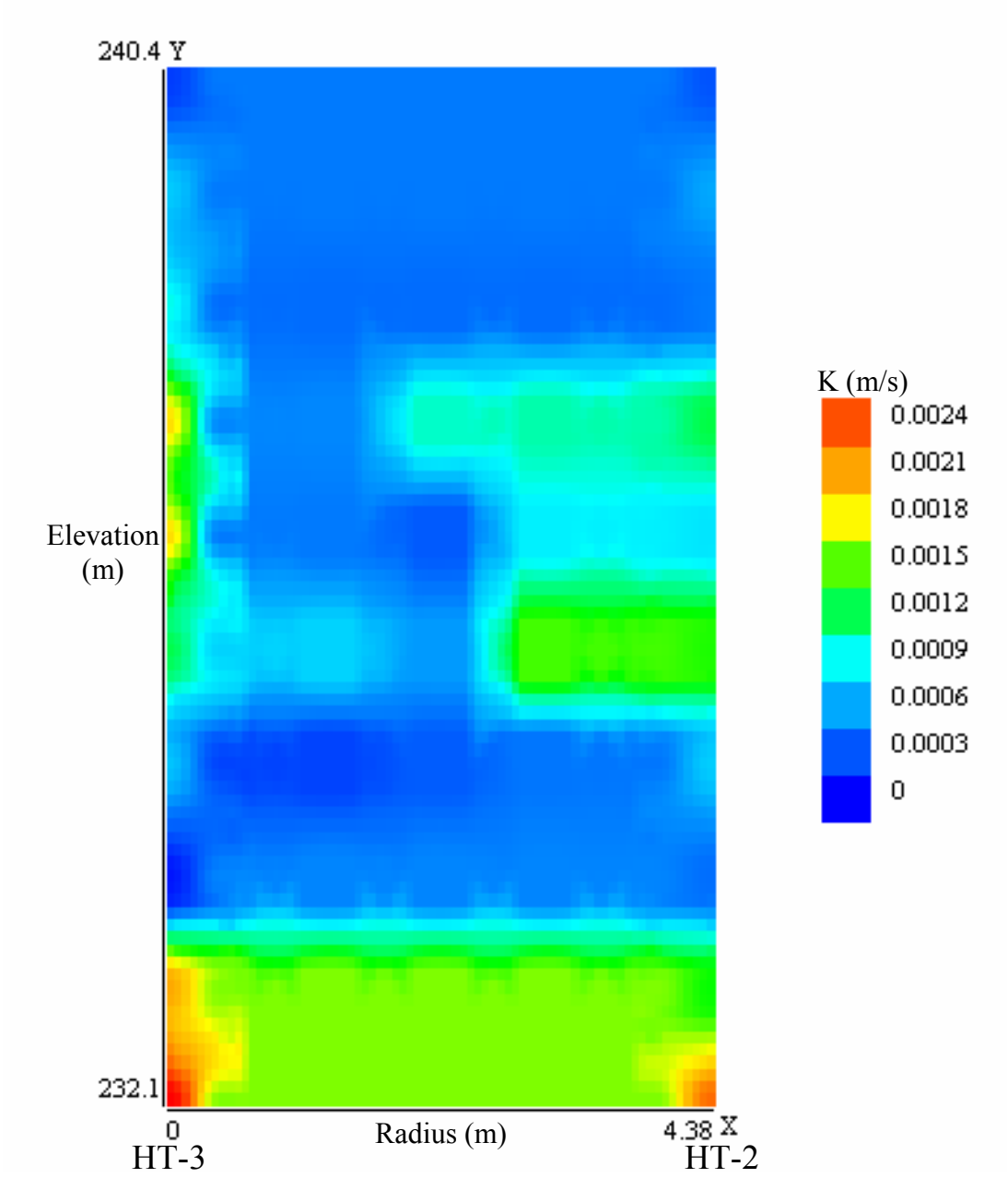

Figure 17: Interwell K values from constrained SVD analysis with HT-3 as the source well and HT-2 as the receiver well (170 rays, $S_s = 10^{-5}$).

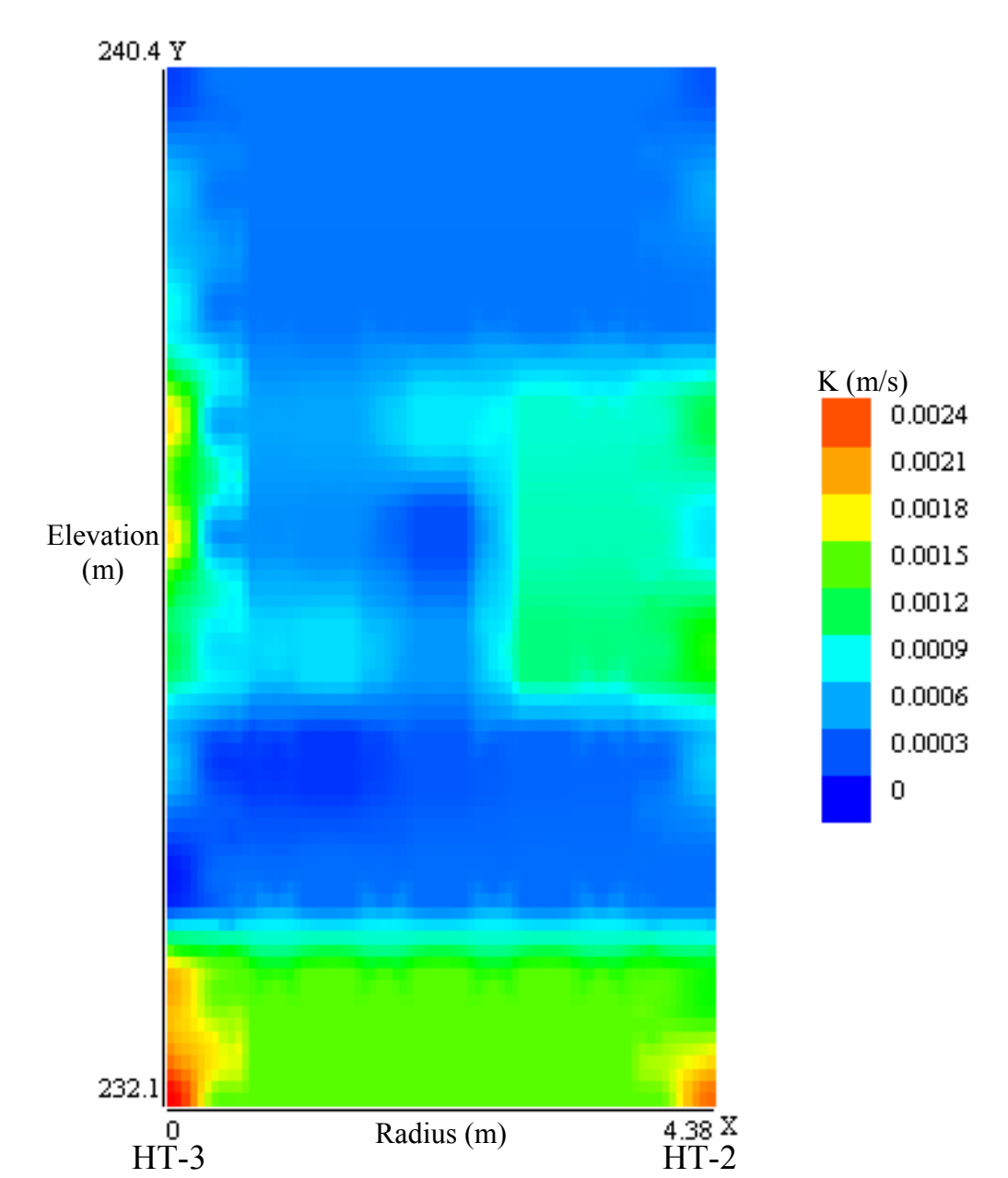

Figure 18: Interwell K values from constrained SVD analysis with HT-3 as the source well and HT-2 as the receiver well (90 rays, $S_s = 10^{-5}$).

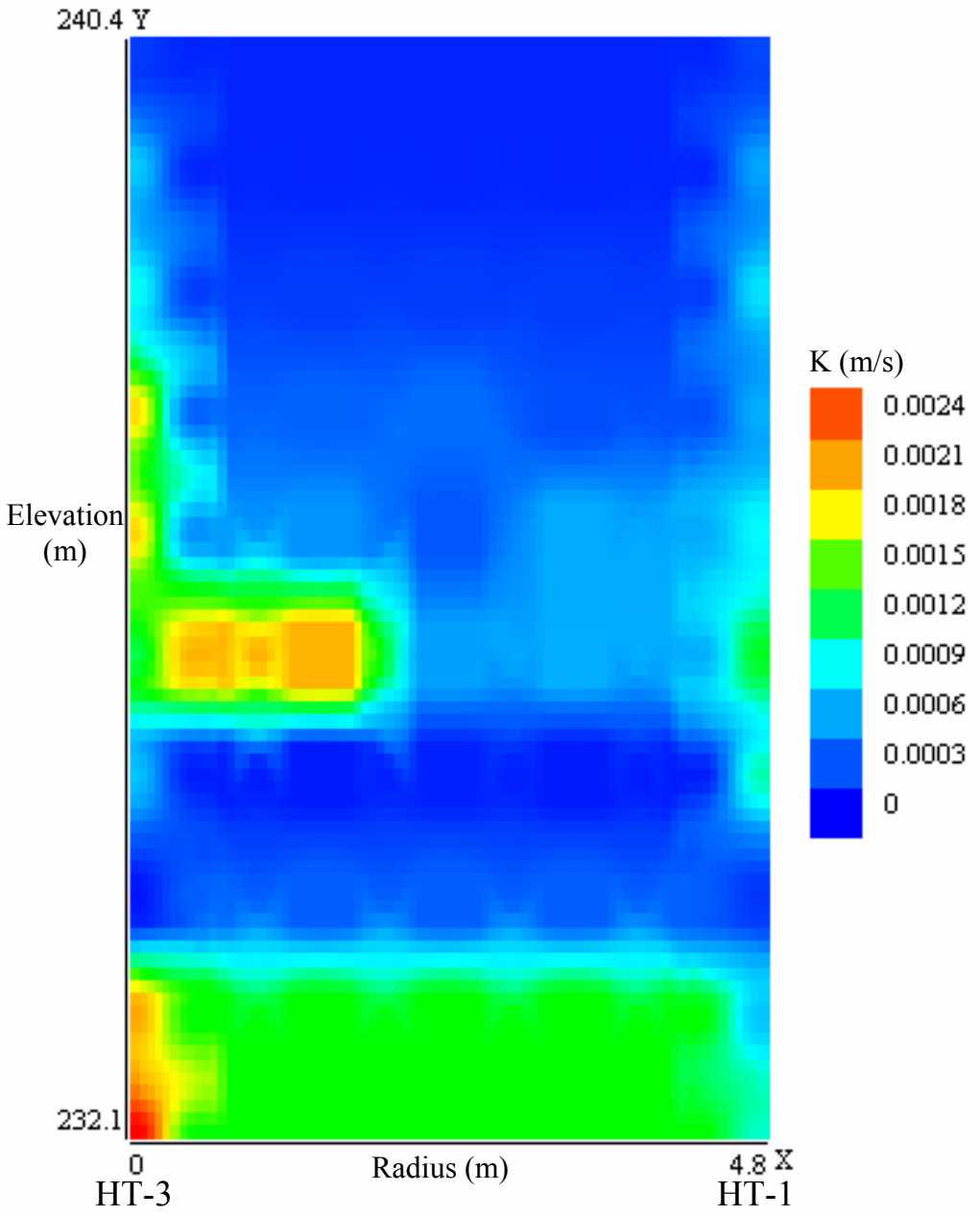

Figure 19: Interwell K values from constrained SVD analysis with HT-3 as the source well and HT-1 as the receiver well ($S_s = 10^{-5}$).

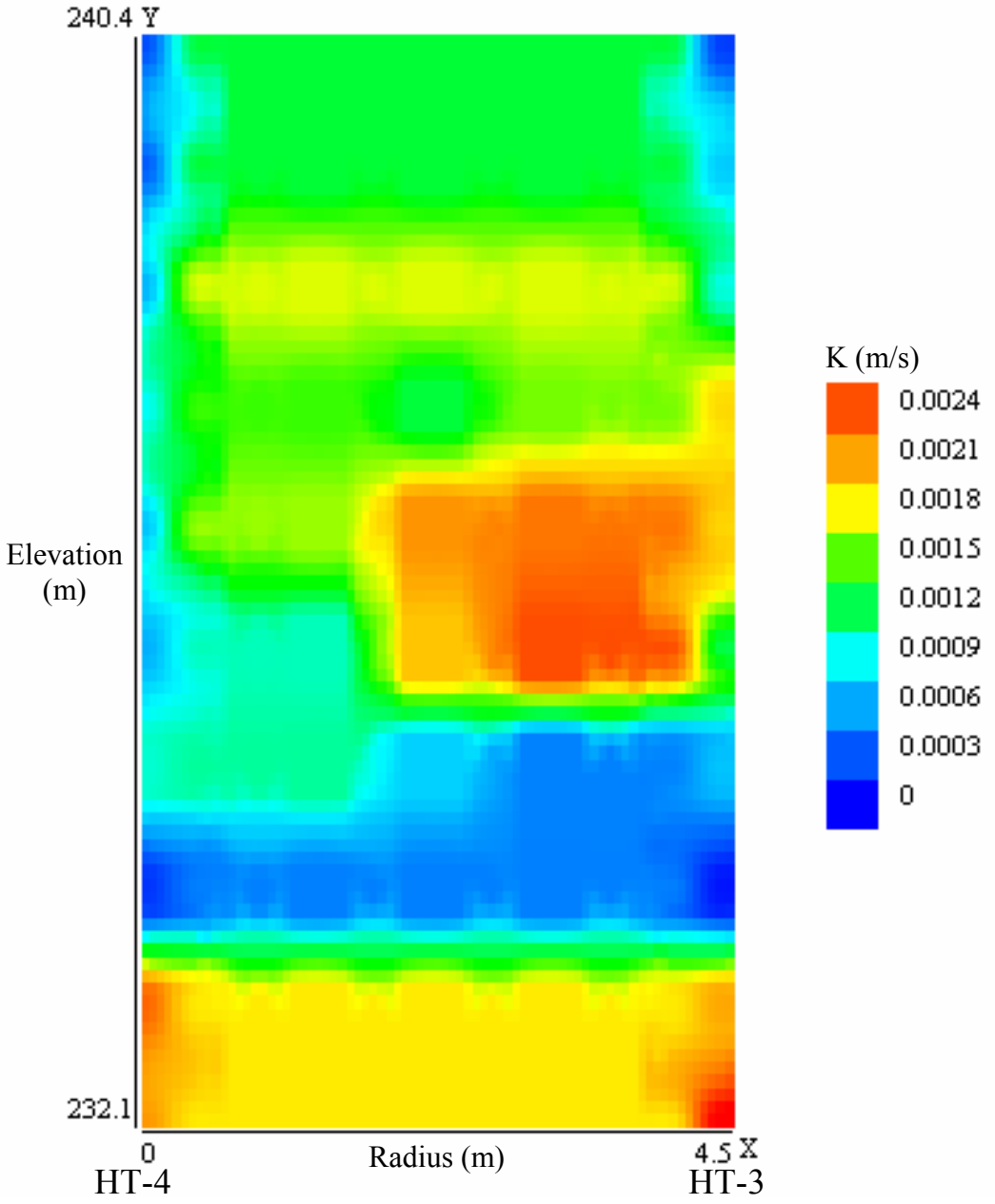

Figure 20: Interwell K values from constrained SVD analysis with HT-4 as the source well and HT-3 as the receiver well ($S_s = 10^{-5}$).

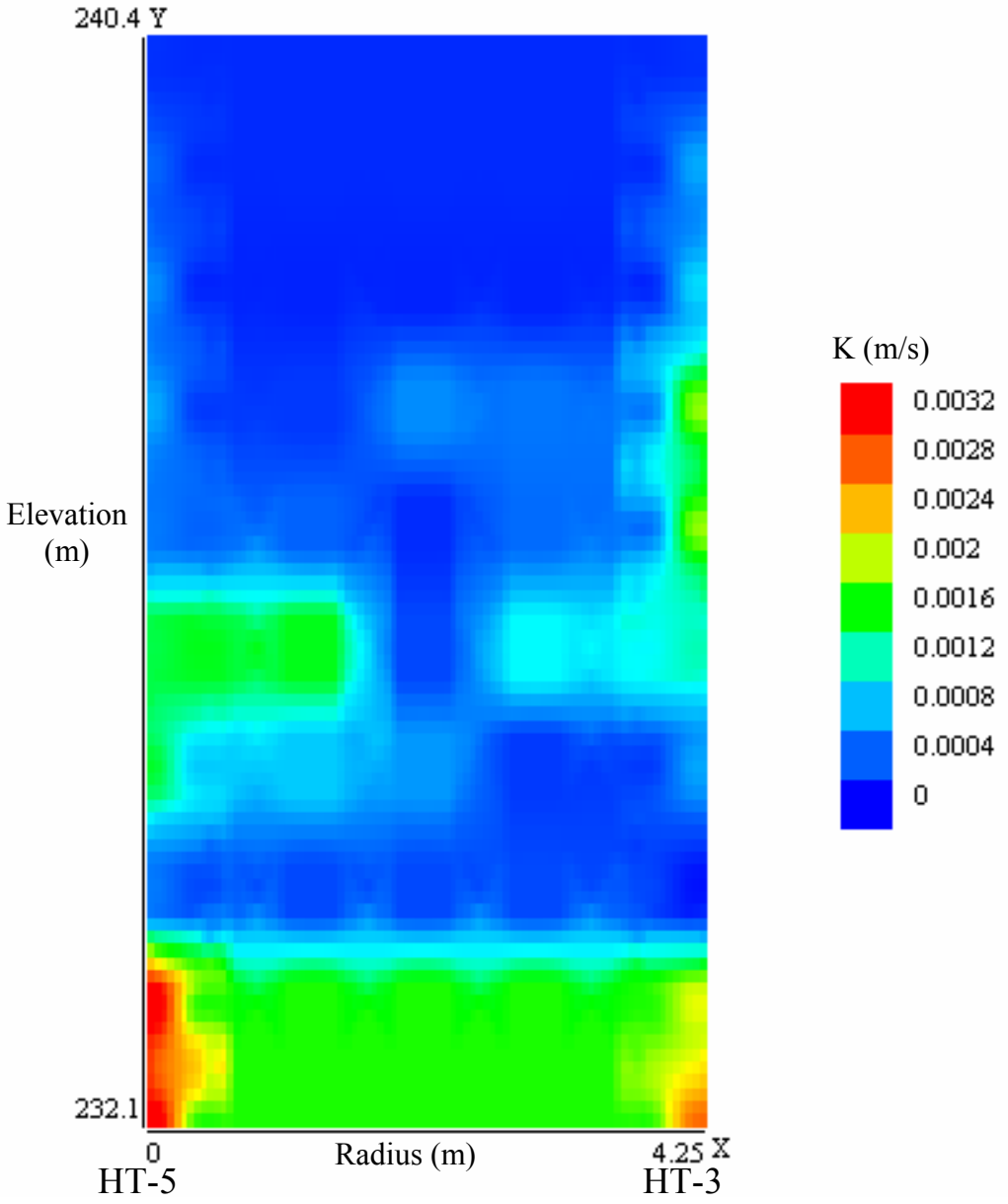

Figure 21: Interwell K values from constrained SVD analysis with HT-5 as the source well and HT-3 as the receiver well ($S_s = 10^{-5}$).

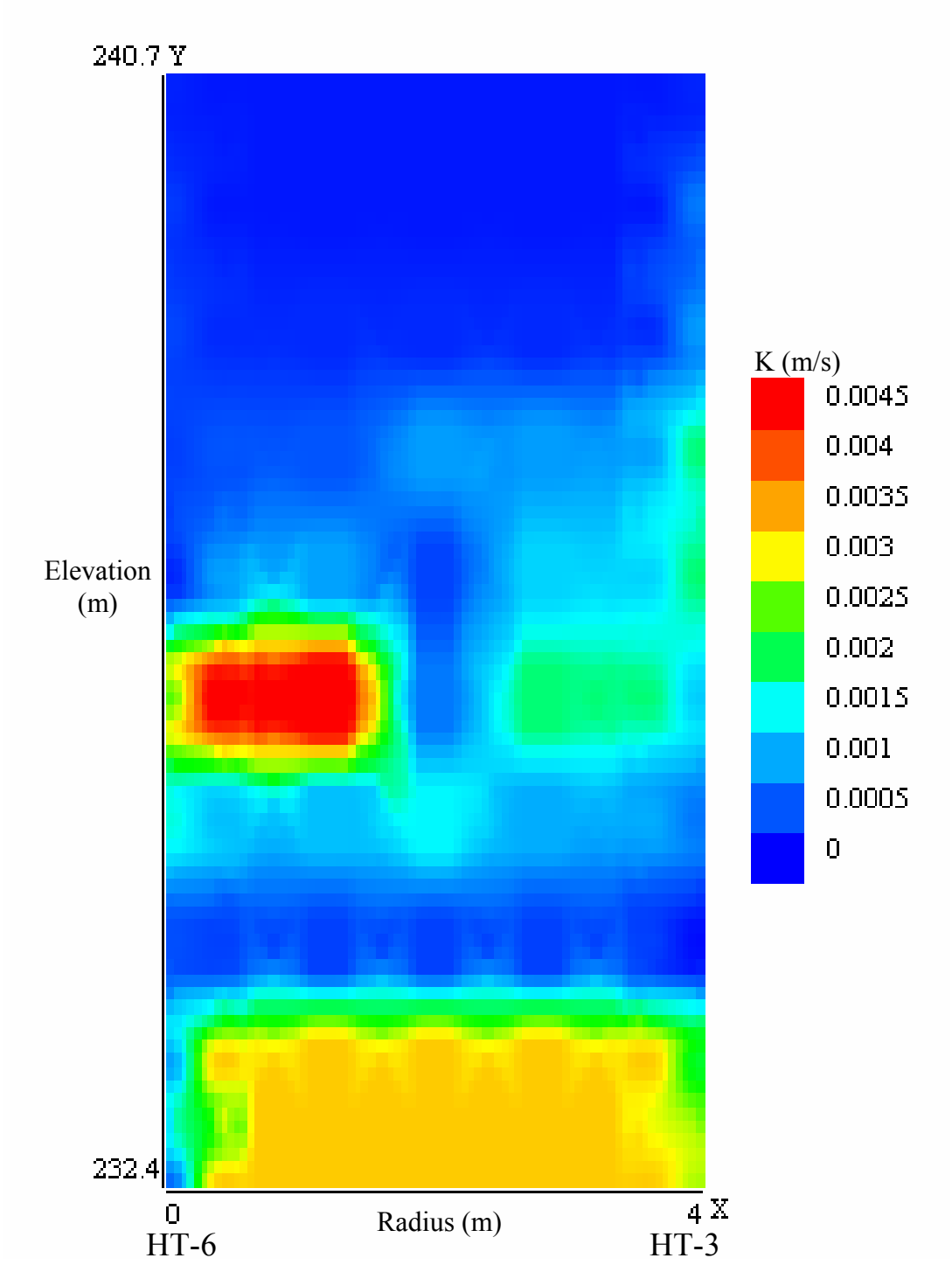

Figure 22: Interwell K values from constrained SVD analysis with HT-6 as the source well and HT-3 as the receiver well ($S_s = 10^{-5}$).

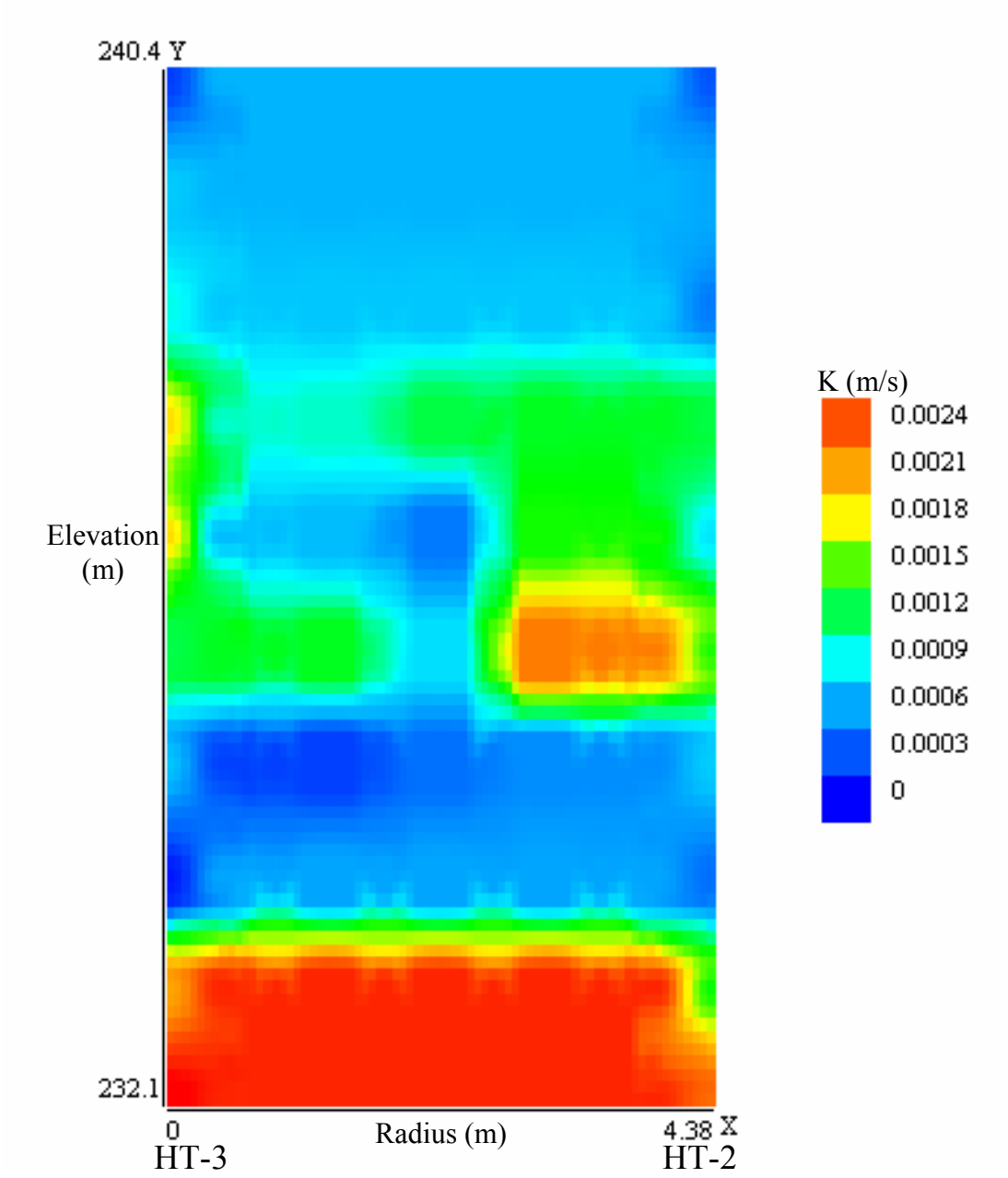

Figure 23: Interwell K values from constrained SVD analysis with HT-3 as the source well and HT-2 as the receiver well (750 rays, $S_s = 1.5 \times 10^{-5}$).

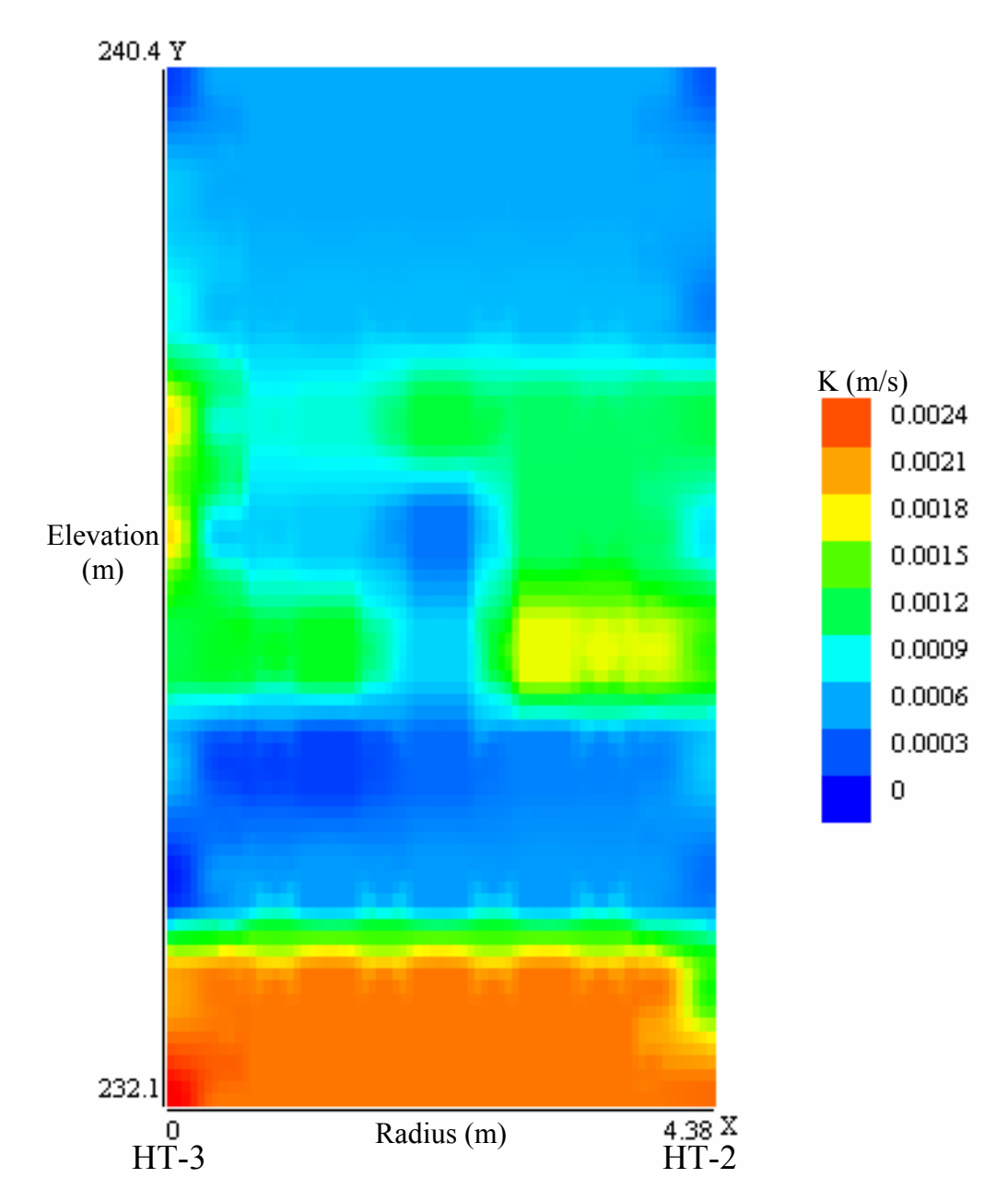

Figure 24: Interwell K values from constrained SVD analysis with HT-3 as the source well and HT-2 as the receiver well (270 rays, $S_s = 1.5 \times 10^{-5}$).

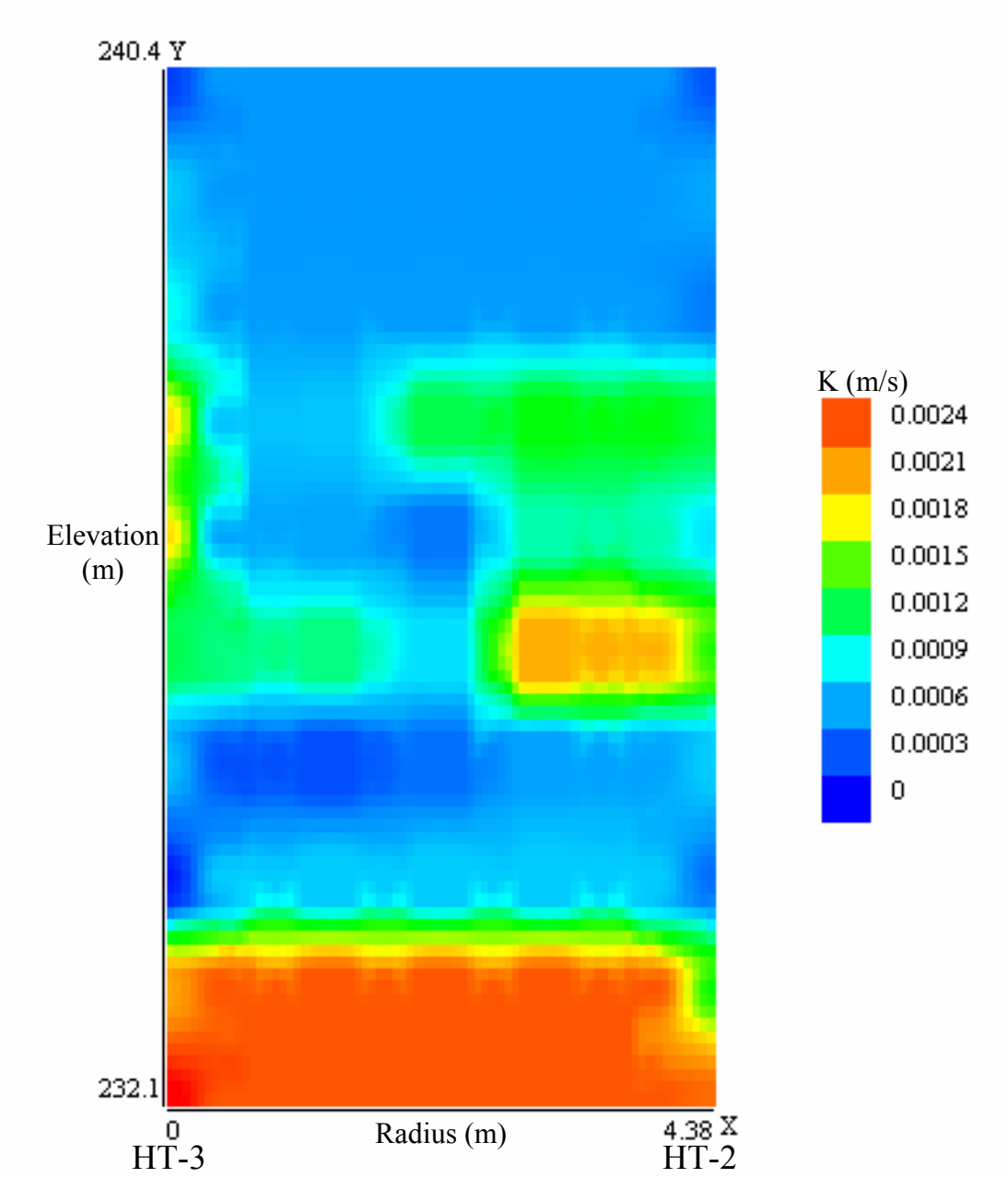

Figure 25: Interwell K values from constrained SVD analysis with HT-3 as the source well and HT-2 as the receiver well (170 rays, $S_s = 1.5 \times 10^{-5}$).

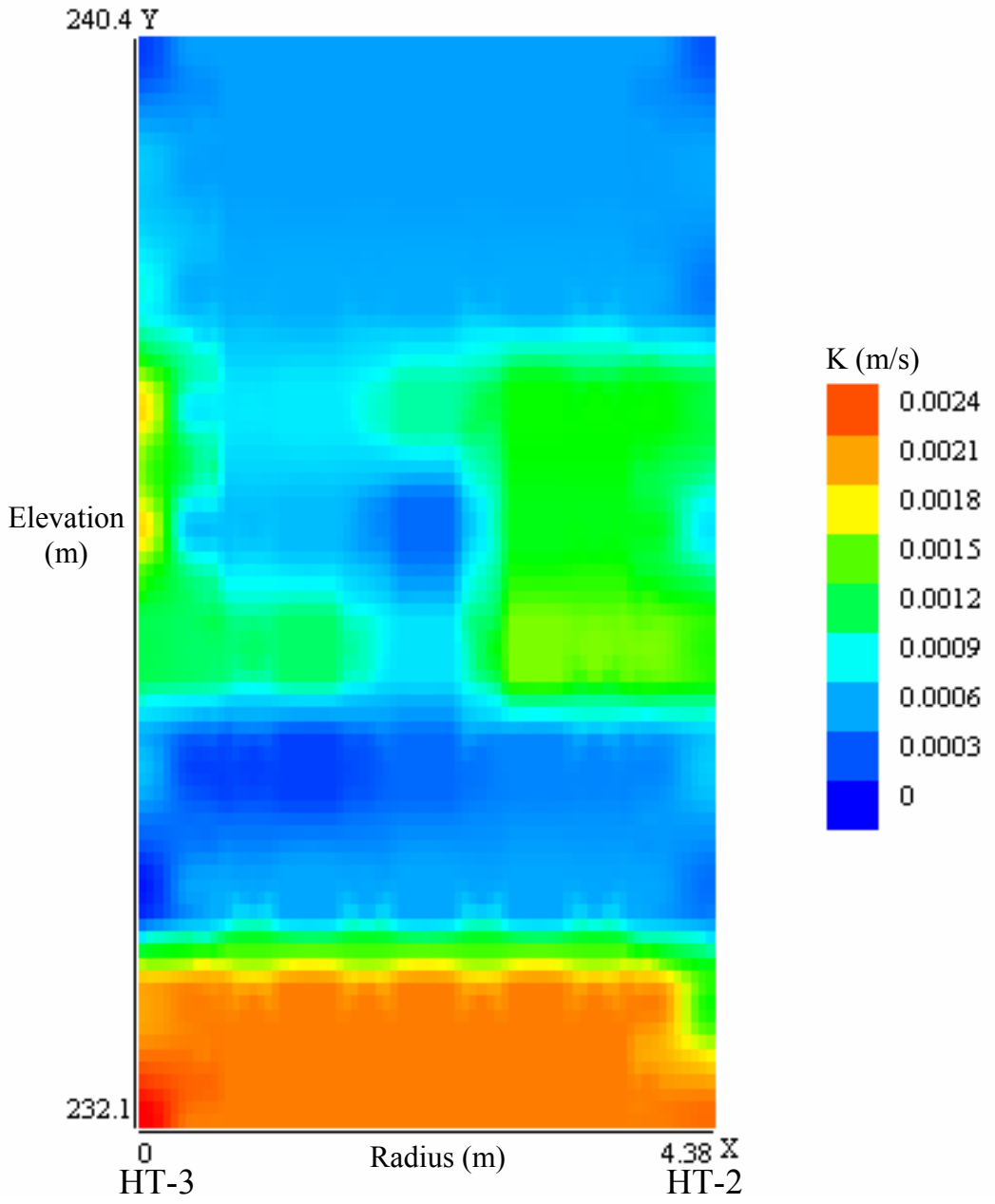

Figure 26: Interwell K values from constrained SVD analysis with HT-3 as the source well and HT-2 as the receiver well (90 rays, $S_s = 1.5 \times 10^{-5}$).

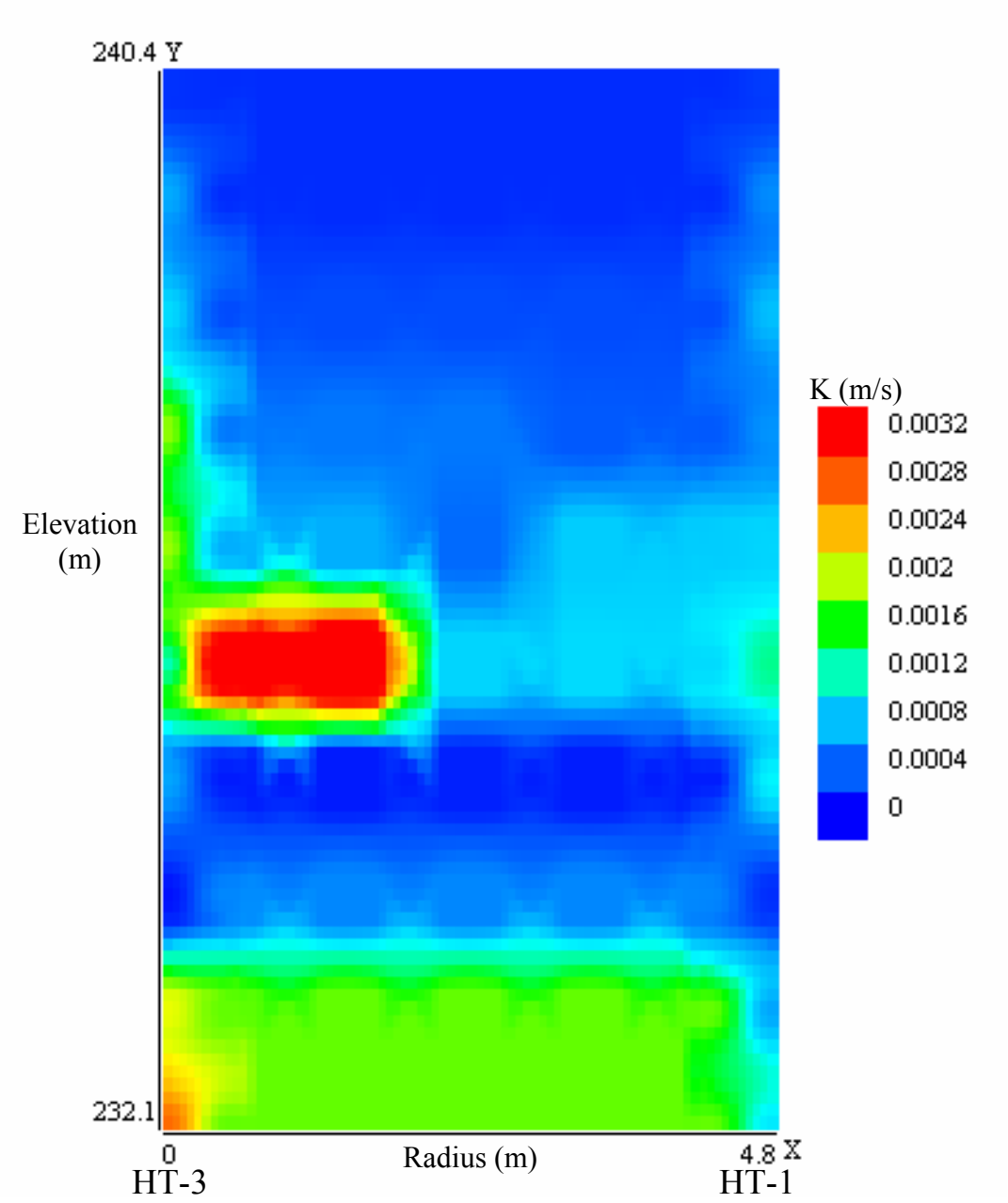

Figure 27: Interwell K values from constrained SVD analysis with HT-3 as the source well and HT-1 as the receiver well ($S_s = 1.5 \times 10^{-5}$).

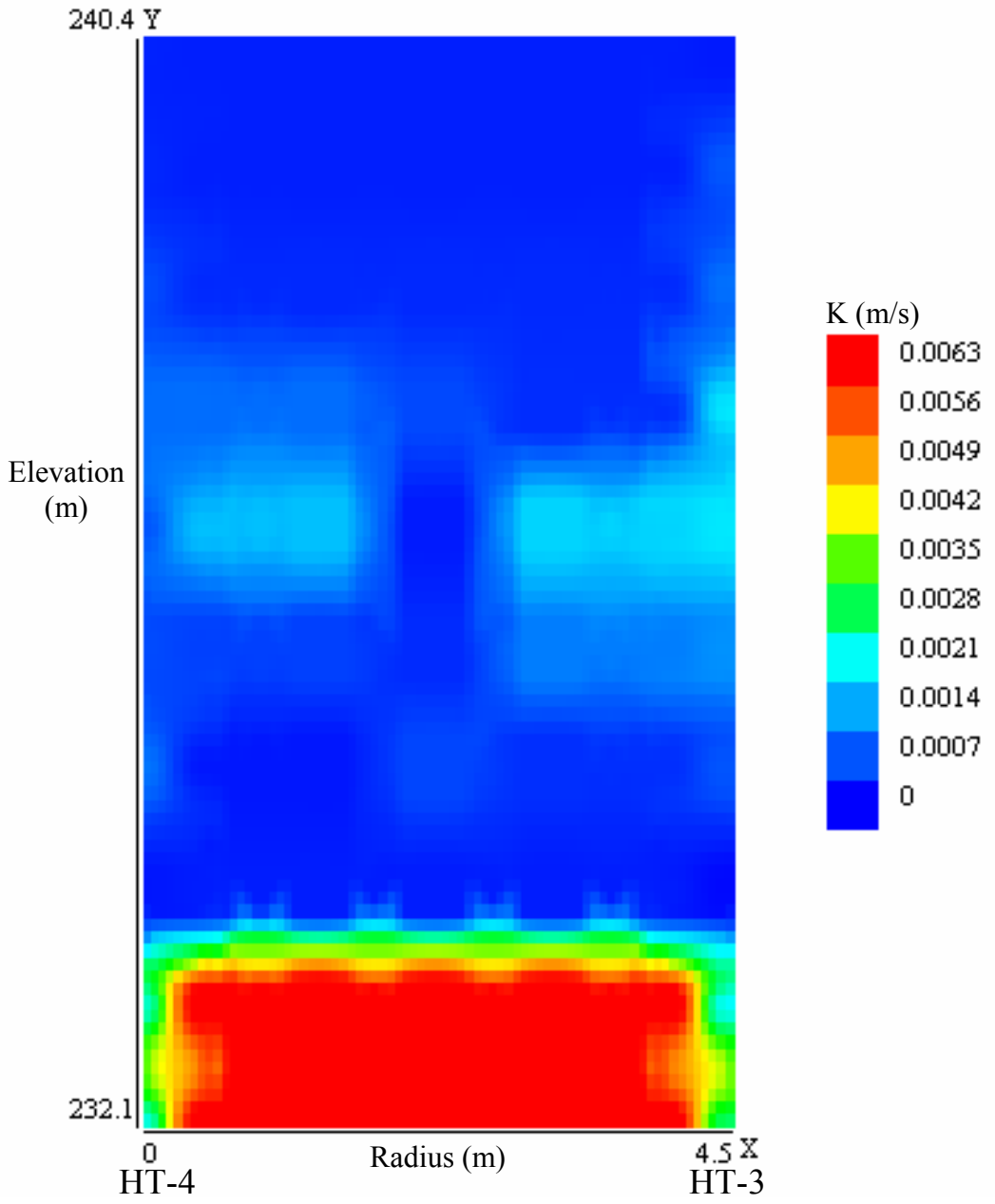

Figure 28: Interwell K values from constrained SVD analysis with HT-4 as the source well and HT-3 as the receiver well ($S_s = 1.5 \times 10^{-5}$).

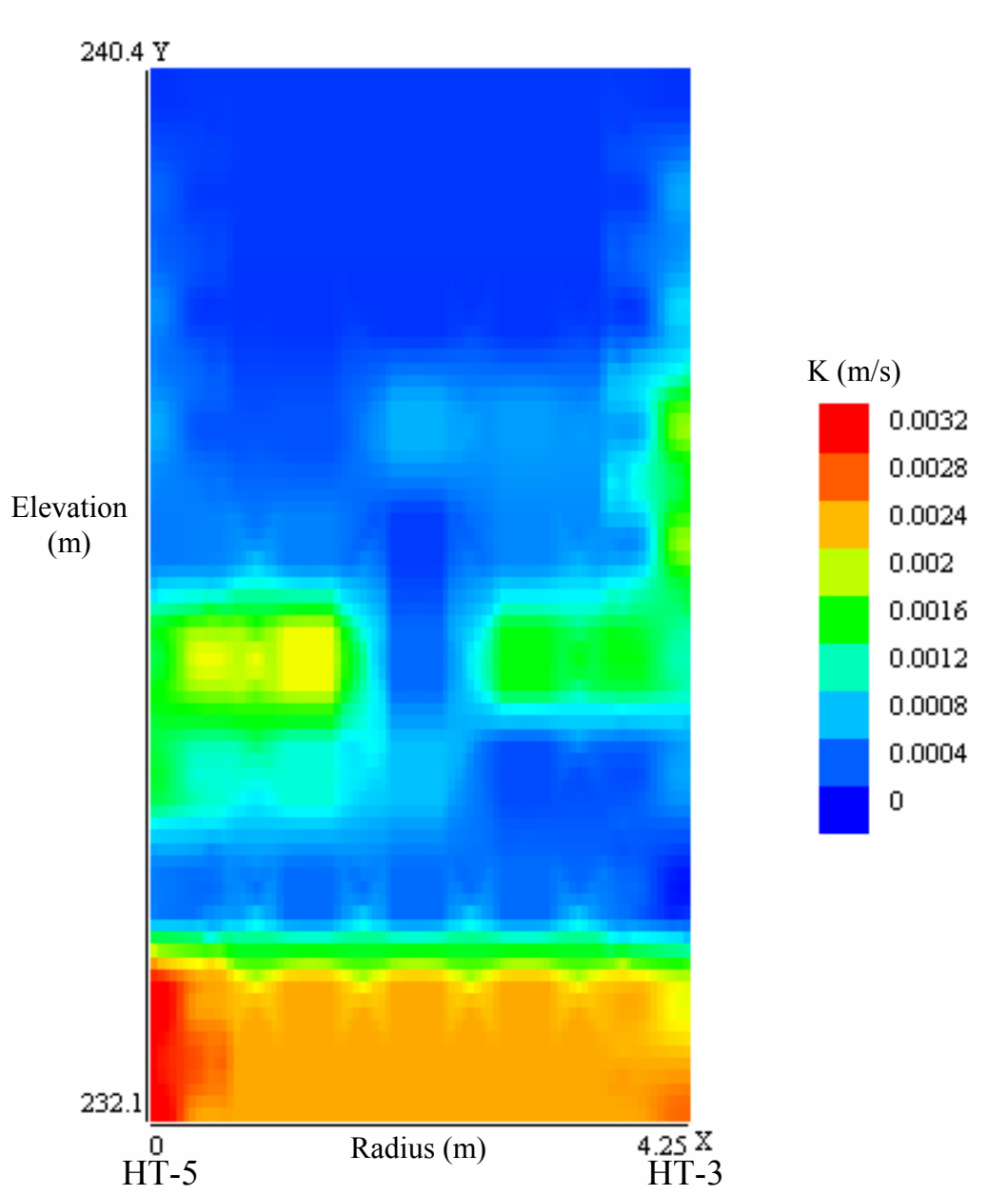

Figure 29: Interwell K values from constrained SVD analysis with HT-5 as the source well and HT-3 as the receiver well ($S_s = 1.5 \times 10^{-5}$).

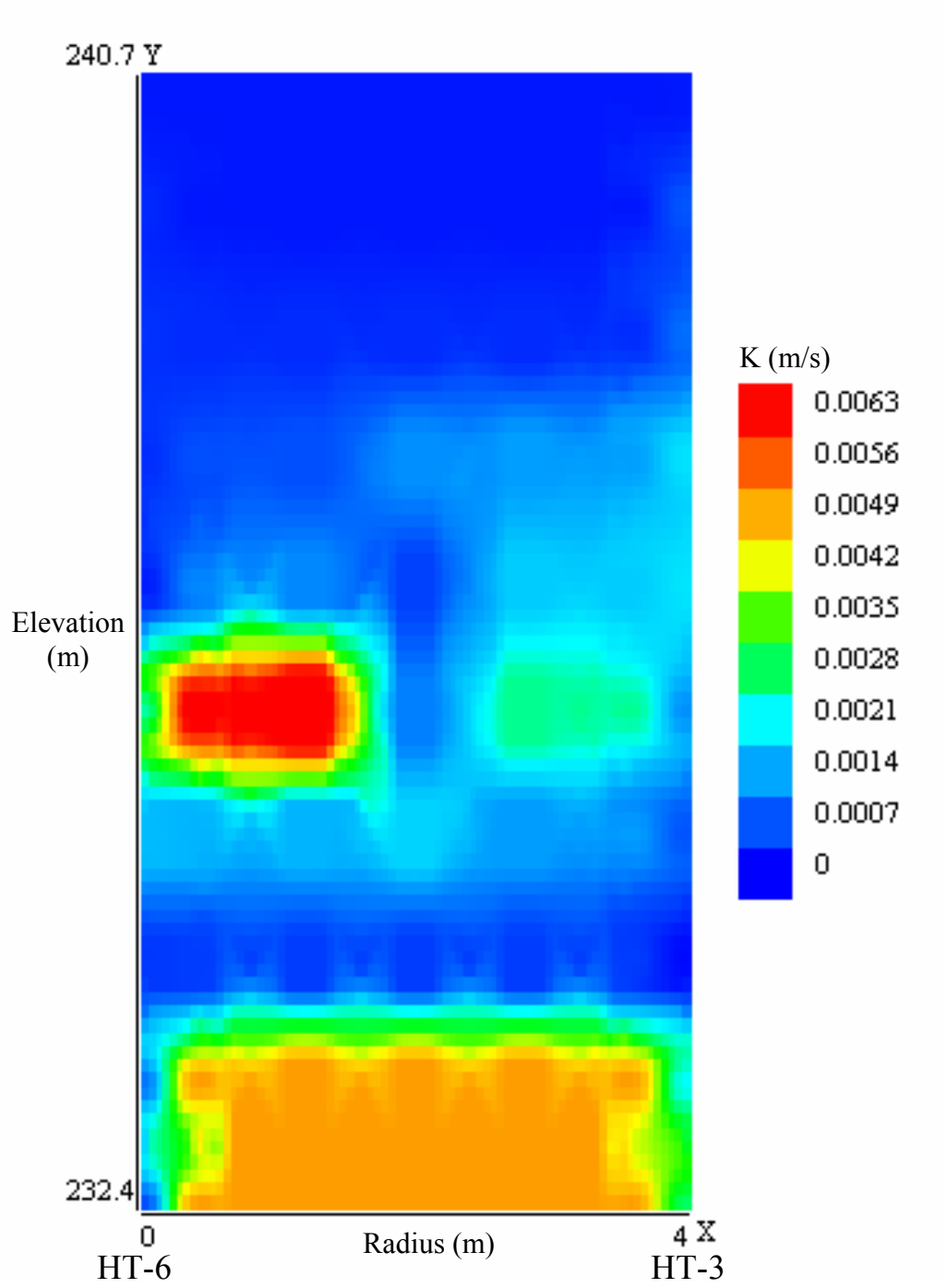

Figure 30: Interwell K values from constrained SVD analysis with HT-6 as the source well and HT-3 as the receiver well ($S_s = 1.5 \times 10^{-5}$).

Summary and Conclusions

The goals of this research were to develop field equipment and time-efficient processing procedures to characterize aquifer parameters using hydraulic tomography with a sinusoidal pressure source. The study consisted of collecting and processing a series of MOGs at a well-studied alluvial aquifer in eastern Kansas. Previous studies at the site focused on obtaining information about K that was specific to the immediate area around the wells, or a large average K value across the entire site. A K value averaged over a large area is useful for water resource problems, but studies at contaminated sites require an understanding of fine-scale heterogeneities in K. Initial data were collected with a single channel receiver, but a multilevel sensor receiver constructed later substantially sped up data collection.

Most hydraulic tomography studies use processing programs that require large amounts of time and processing power for the inversion to K values. The straight ray trace approximation greatly simplifies the processing. The unconstrained SVD inversion program was created and modeling studies were performed using synthetic data to demonstrate that data could be inverted with relatively small amounts of error. Zones could be resolved using the SVD program to dimensions of about one meter. After modeling, the SVD program was run using phase values obtained in the field. K values at the site are known from HRST to range from about 0.000305 m/s to 0.00305 m/s, and follow the general trend of higher K zone at the base of the aquifer, a low K zone above, a moderately high K zone still higher up the profile, and a low K zone at the top. The success or failure of the inversion was evaluated by comparing the resulting K values to the range of K values seen from HRST as well as the general trends of high or low K

zones seen from HRST. The unconstrained analysis showed the general trends from the site, but some K values were orders of magnitude above the expected range. Filtering and editing of rays failed to reduce the magnitude of K values into the expected range. The SVD analysis program was then updated with a weighting factor for HRST results used to constrain the inversion. The constrained SVD analysis produced both the expected trends of high and low K zones as well as K values within the expected range.

The success of the inversion seems to be correlated with the number of ray paths between the source and receiver wells. Varying source and receiver intervals for each well pair offered the opportunity to examine how much data needed to be collected. Initial data were collected at too fine a scale (0.305 m) given the resolution capabilities of the model, yet two of the later well pairs did not have enough ray paths to adequately characterize the area (using a 0.914 m collection interval). Varying the number of ray paths used in the initial well pair verified this conclusion. Of the variations tested in this study, the geometry used for GEMS was most efficiently and accurately characterized with 300 ray paths, but 750 ray paths will provide some additional accuracy if time is available for their collection.

The goals of the research were successfully achieved. The newly developed field equipment and processing programs reduced the time to get K values from a hydraulic tomography study. Five well pairs were analyzed and all had reasonable interwell K distributions after using the constrained inversion, compared to the general range seen with HRST. The small problems with some well pairs can be explained by equipment problems in one case and by too few ray paths in two cases. This research shows that hydraulic tomography combined with appropriate inversion programs can estimate

interwell K distributions with resolutions of about one square meter in the most sensitive regions. This research was supported in part by the U.S. Department of Defense, through the Strategic Environmental Research and Development Program (SERDP).

References

Aster, R.C., Borchers, B., and Thurber, C.H., 2005, Parameter Estimation and Inverse Problems, Elsevier Academic Press, Burlington, MA.

Barker, J.A., 1988. A generalized radial flow model for hydraulic tests in fractured rock. *Water Resources Research* 24. No. 10:1796-1804.

Black, J.H., and Kipp, K.L. 1981. Determination of hydrogeological parameters using sinusoidal pressure tests: A theoretical appraisal. *Water Resources Research* 17. No. 3:686-692.

Bohling, G.C., 1999. Evaluation of an induced gradient tracer test in an alluvial aquifer, Ph.D. Dissertation, University of Kansas, 224 p.

Bohling, G.C., Zhan, X., Knoll, M.D., Butler J.J. Jr. 2003. Hydraulic tomography and the impact of a priori information: An alluvial Aquifer Example. *Kansas Geological Survey Open-file Report 2003-71*

Brauchler, R., Liedl, R., Dietrich, P., 2001. A travel time based hydraulic tomographic approach. *Water Resources Research* 39. No. 12:1-12

Bredehoeft, J.D and Papadopulos, S.S. 1980. A method for determining the hydraulic properties of tight formations. *Water Resources Research* 16. No. 1:233-238

Cooper, H.H., Bredehoeft, J.D., Papadopulos, I.S., and Bennett, R.R. 1965. The response of well-aquifer systems to seismic waves. *Journal of Geophysical Research* 70, No. 16:3915-3926

Engard, B., 2006, Estimating Aquifer Parameters From Horizontal Pulse Tests, Masters Thesis, University of Kansas, 107 pp.

Engard, B., McElwee, C.D., Healey, J.M., and Devlin, J.F., 2005, Hydraulic tomography and high-resolution slug testing to determine hydraulic conductivity distributions – Year 1: Kansas Geological Survey Open File Report #2005-36, 81 p.

Engard, B.R., McElwee, C.D., Devlin, J.F., Wachter, B., and Ramaker, B., 2006, Hydraulic tomography and high-resolution slug testing to determine hydraulic conductivity distributions – Year 2: Kansas Geological Survey Open-File Report # 2007-5, 57 pp.

Ferris, J.G., 1951. Cyclic fluctuations of the waterlevels as a basis for determining aquifer transmissivity, IAHS *Publ.,* 33, p. 148-155.

Hantush, M.S., 1960. Lectures at New Mexico Institute of Mining and Technology. unpublished, compiled by Steve Papadopulos, 119 p.

Healey, J., McElwee, C., and Engard, B., 2004. Delineating hydraulic conductivity with direct-push electrical conductivity and high resolution slug testing. *Trans. Amer. Geophys. Union* 85, No.47: Fall Meet. Suppl., Abstract H23A-1118.

Huettl, T.J., 1992. An evaluation of a borehole induction single-well tracer test to characterize the distribution of hydraulic properties in an alluvial aquifer. Masters Thesis, The University of Kansas.

Jiang, X., 1991. Field and laboratory study of the scale dependence of hydraulic conductivity. Masters Thesis, The University of Kansas.

Jiao, J.J. and Tang, Z., 1999. An analytical solution of groundwater response to tidal fluctuation in a leaky confined aquifer. *Water Resources Research* 35. No. 3:747-751

Johnson, C.R., Greenkorn, R.A., and Woods, E.G., 1966. Pulse-Testing: A new method for describing reservoir flow properties between wells. *Journal of Petroleum Technology.* (Dec1966) pp. 1599-1601.

Lee, J., 1982. Well Testing. Society of Petroleum Engineers of AIME, New York. 156 p.

McCall, W., Butler J.J. Jr., Healey, J.M., and Garnett, E.J., 2000. A dual-tube direct push method for vertical profiling of hydraulic conductivity in unconsolidated formations. *Environmental & Engineering Geoscience* Vol. VIII, no. 2:75-84.

McElwee, C.D., 2000, Implementation of a nonlinear model for analysis of slug tests, Kansas Geological Survey Computer Program Series 2000-01.

McElwee, C.D., 2001. Application of a nonlinear slug test model. *Ground Water* 39. No. 5:737-744.

McElwee, C.D., 2002. Improving the analysis of slug tests. *Journal of Hydrology* 269:122-133.

McElwee, C.D., and Butler, J.J. Jr., 1995. Characterization of heterogeneities controlling transport and fate of pollutants in unconsolidated sand and gravel aquifers: Final report. Kansas Geological Survey open file report 95-16.

McElwee, C.D., and Zenner, M.A., 1998. A nonlinear model for analysis of slug-test data. *Water Resources Research* 34. No. 1:55-66.

Novakowski, K.S., 1989. Analysis of pulse interference tests. *Water Resources Research* 25. No. 11:2377-2387

Pierce, A., 1977. Case history: Waterflood perfomance predicted by pulse testing. *Journal of Petroleum Technology.* (August 1977) 914-918.

Ross, H.C. 2004. Utility of multi-level slug tests to define spatial variations of hydraulic conductivity in an alluvial aquifer, northeastern Kansas. Masters Thesis, The University of Kansas.

Ross, H.C. and McElwee, C.D., 2007, Multi-level slug tests to measure 3-D hydraulic conductivity distributions. *Natural Resources Research*, DOI: 10.1007/s11053-007-9034-9.

Schad, H., and Teutsch, G., 1994. Effects of scale on pumping test results in heterogeneous porous aquifers. *Journal of Hydrology* 159. pp. 61- 77.

Schulmeister, 2000. Hydrology and geochemistry of an alluvial aquifer near a flood plain margin. Dissertation, University of Kansas.

Sellwood, S., 2001. A direct-push method of hydrostratigraphic site characterization. Masters thesis, The University of Kansas.

Van Der Kamp, G.,1976. Determining aquifer transmissivity by means of whole well respons tests: The underdamped case. *Water Resources Research* 12. No. 1:71-77.

Yeh, T.C., and Liu, S., 2000. Hydraulic tomography: Development of a new aquifer test method. *Water Resource Research* 36. No. 8:2095-2105

Zemansky, G.M., and McElwee, C.D., 2005. High-Resolution Slug Testing. *Ground Water* 43. No. 2: 222-230

Appendix A. Technical Publications

Published Abstracts.

Healey, J. M., McElwee, C. D., and Engard, B., 2004, Delineating hydraulic conductivity with direct push electrical conductivity and high-resolution slug testing: *Eos, Trans. Amer. Geophys. Union*, v. 85, no 47, Fall Meet. Suppl., Abstract H23A-1118, p. F773.

Engard, B. and McElwee, C. D., 2005, Continuous pulse testing for estimating aquifer parameters: *Proceedings 50th Annual Midwest Ground Water Conference*, Nov. 1-3, Urbana, Illinois.

Engard, B. and McElwee, C. D., 2005, Estimating aquifer parameters from oscillatory well stresses: *Proceedings SERDP Partners in Environmental Technology Technical Symposium and Workshop*, Nov. 29-Dec. 1, Washington, D.C., p. G-26.

Engard, B. and McElwee, C. D., 2005, Estimating hydraulic conductivity: Hydraulic tomography and high-resolution slug tests: *Eos, Trans. Amer. Geophys. Union*, 86(52), Fall Meet. Suppl., Abstract H21C-1359.

McElwee, C. D. and Engard, B., 2006, Using Oscillatory Pressure Waves to Measure Hydraulic Conductivity Distributions: *Proceedings SERDP Partners in Environmental Technology Technical Symposium and Workshop*, Nov. 28-30, Washington, D.C.

McElwee, C. D. and Engard, B., 2006, Hydraulic Tomography Using Oscillatory Pressure Waves: *Eos, Trans. Amer. Geophys. Union*, 87(52), Fall Meet. Suppl., Abstract H41B-0382.

McElwee, C. D., 2007, Hydraulic Conductivity Distributions from Pulsed Signals: Mini-Symposium 45 – Tomographic Approaches to High-Resolution Aquifer Characterization – Lab and Field Experiments, SIAM Conference on Mathematical & Computational Issues in the Geosciences, March 19-22, Santa Fe, NM.

McElwee, C. D. and Wachter, B. J., 2007, A Modeling Study Using Oscillatory Pressure Waves for Hydraulic Tomography: *Eos, Trans. Amer. Geophys. Union*, 88(23), Joint Assembly Suppl., Abstract H51E-01.

McElwee, C. D. and Wachter, B. J., 2007, Oscillatory Pressure Waves as Energy Source for Hydraulic Tomography: *Proceedings SERDP Partners in Environmental Technology Technical Symposium and Workshop*, Dec. 4-6, Washington, D.C.

Wachter, B. J. and McElwee, C. D., 2007, Hydraulic Tomography Study Involving the Singular Value Decomposition Method: *Eos, Trans. Amer. Geophys. Union*, 88(52), Fall Meet. Suppl., Abstract H23G-1725.

McElwee, C. D. and Wachter, B. J., 2008, Characterizing Aquifer Heterogeneity Using Hydraulic Tomography with a Sinusoidal Signal: *Proceedings SERDP Partners in Environmental Technology Technical Symposium and Workshop*, Dec. 2-4, Washington, D.C.

McElwee, C. D. and Wachter, B. J., 2008, Hydraulic Tomography Using A Sinusoidal Signal To Characterize Aquifer Hydraulic Conductivity: *Eos, Trans. Amer. Geophys. Union*, 89(53), Fall Meet. Suppl., Abstract H41A-0827.

Annual Report

Engard, B., McElwee, C.D., Healey, J.M., and Devlin, J.F., 2005, Hydraulic tomography and high-resolution slug testing to determine hydraulic conductivity distributions – Year 1, Project Report to the Strategic Environmental Research and Development Program, U.S. DoD, EPA, and DOE, 81 pp., also Kansas Geological Survey Open File Report #2005-36.

Engard, B.R., McElwee, C.D., Devlin, J.F., Wachter, B., and Ramaker, B., 2006, Hydraulic tomography and high-resolution slug testing to determine hydraulic conductivity distributions – Year 2, Project Report to the Strategic Environmental Research and Development Program, U.S. DoD, EPA, and DOE, 57 pp., also Kansas Geological Survey Open-File Report # 2007-5.

McElwee, C.D., Devlin, J.F., and Wachter, B., 2007, Hydraulic tomography and high-resolution slug testing to determine hydraulic conductivity distributions – Year 3, Project Report to the Strategic Environmental Research and Development Program, U.S. DoD, EPA, and DOE, 57 pp., also Kansas Geological Survey Open-File Report # 2008-1.

Masters Thesis

Engard, B., 2006, Estimating Aquifer Parameters From Horizontal Pulse Tests, Masters Thesis, University of Kansas, 107 pp.

Wachter, B., 2007, Characterizing Aquifer Heterogeneity Using Hydraulic Tomography, Masters Thesis, University of Kansas, 150 pp.